(2)

TECHNICAL REPORT RD-RE-88-4

DIGITAL PROCESSING OF SPECKLE IMAGES

Charles R. Christensen
Research Directorate
Research, Development, & Engineering Center

and

Anil K. Jain
JMA, Inc.
517 Hubble Street
Davis, CA 95616

APRIL 1988

U.S. ARMY MISSILE COMMAND
Redstone Arsenal, Alabama 35898-5000

Approved for public release; distribution is unlimited.

REPORT DOCUMENTATION PAGE

Form Approved
OMB No 0704-0188
Exp Date Jun 30, 1986

1a REPORT SECURITY CLASSIFICATION UNCLASSIFIED	1b. RESTRICTIVE MARKINGS
2a. SECURITY CLASSIFICATION AUTHORITY	3. DISTRIBUTION / AVAILABILITY OF REPORT Approved for public release; distribution is unlimited.
2b. DECLASSIFICATION / DOWNGRADING SCHEDULE	
4 PERFORMING ORGANIZATION REPORT NUMBER(S) TR-RD-RE-88-4	5. MONITORING ORGANIZATION REPORT NUMBER(S)
6a. NAME OF PERFORMING ORGANIZATION Research Directorate Res, Dev, & Eng (RD&E) Center 6b. OFFICE SYMBOL (If applicable) AMSMI-RD-RE	7a. NAME OF MONITORING ORGANIZATION
6c. ADDRESS (City, State, and ZIP Code) Commander U.S. Army Missile Command, ATTN: AMSMI-RD-RE Redstone Arsenal, AL 35898-5248	7b. ADDRESS (City, State, and ZIP Code)
8a. NAME OF FUNDING / SPONSORING ORGANIZATION 8b. OFFICE SYMBOL (If applicable)	9. PROCUREMENT INSTRUMENT IDENTIFICATION NUMBER
8c. ADDRESS (City, State, and ZIP Code)	10. SOURCE OF FUNDING NUMBERS PROGRAM ELEMENT NO. / PROJECT NO. / TASK NO / WORK UNIT ACCESSION NO

11 TITLE (Include Security Classification)
DIGITAL PROCESSING OF SPECKLE IMAGES

12. PERSONAL AUTHOR(S)
Anil K. Jain (JMA, Inc.) and Charles R. Christensen (Research Directorate)

13a. TYPE OF REPORT	13b. TIME COVERED	14. DATE OF REPORT (Year, Month, Day)	15. PAGE COUNT
Final	FROM _____ TO Jan 88	APRIL 1988	48

16. SUPPLEMENTARY NOTATION

17 COSATI CODES		
FIELD	GROUP	SUB-GROUP

18. SUBJECT TERMS (Continue on reverse if necessary and identify by block number)
digital processing, linear filter, low pass filtering, speckle noise, median filter, Wiener filter, homomorphic filter, spatial averaging

19. ABSTRACT (Continue on reverse if necessary and identify by block number)

A digital simulation of an image with speckle noise from coherent illumination was developed and verified by comparison with experimentally obtained imagery. The digital simulation was then used to obtain detection probability statistics and to evaluate the utility of several digital filtering techniques for speckle reduction. Homomorphic Wiener filtering produced the best noise reduction with the least degradation in image resolution.

20 DISTRIBUTION / AVAILABILITY OF ABSTRACT ☐ UNCLASSIFIED/UNLIMITED ☒ SAME AS RPT ☐ DTIC USERS	21 ABSTRACT SECURITY CLASSIFICATION UNCLASSIFIED
22a NAME OF RESPONSIBLE INDIVIDUAL Charles R. Christensen	22b TELEPHONE (Include Area Code) (205) 876-3934 22c OFFICE SYMBOL AMSMI-RD-RE

DD FORM 1473, 84 MAR 83 APR edition may be used until exhausted
All other editions are obsolete

TABLE OF CONTENTS

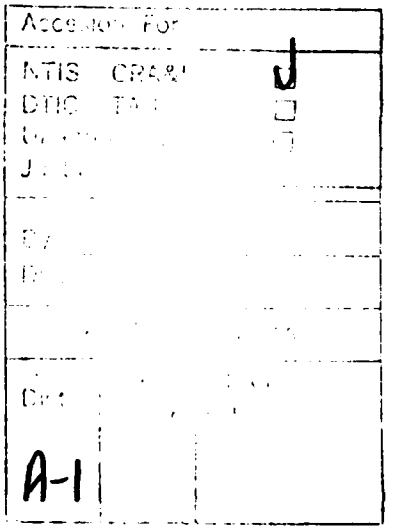

LIST OF FIGURES

LIST OF FIGURES (Concluded)

I. INTRODUCTION

Images obtained using coherent illumination contain a multiplicative noise component called speckle. The noise component is a result of interference between wavelets scattered from a surface whose roughness is on the order of the wavelength of the illumination. The statistical properties of this noise have been developed [1] and the phenomenon and its suppression have been extensively studied [2].

The presence of speckle noise in an imaging system reduces the resolution capability of the system by as much as a factor of seven [3] and is particularly severe in imagery of low contrasts [4]. Thus the suppression of speckle noise is an important component of a coherent imaging system design. The design of suppression techniques can best be optimized by basing them on a detection theory. An excellent account of the detection theory for small high contrast objects in speckle noise has been given by Dainty [5].

For images in speckle, the resolution can be expected to improve if independent intensity patterns, or looks, are superimposed. This is due to the fact that the standard deviation of the mean of N-independent measurement sets is given by $\sigma = \sigma_1/(N)^{1/2}$ where σ_1 is the standard deviation of a single measurement set. The noise can also be reduced by averaging the fluctuations over some area A of uniform intensity in the image. If s is linear dimension of a speckle in the image plane, then the standard deviation should be reduced by a factor proportional to $s/A^{1/2}$.

The procedures used to produce the final speckle smoothed image can be divided into four categories: 1) reduction in the temporal coherence of the illumination, 2) reduction in the spatial coherence of the illumination, 3) time averaging while moving the receiver or transmitter aperture, and 4) integrating adjacent pixels. These techniques trade off system bandwidth, recording time, or system resolution for signal-to-noise improvement.

An appealing option to the above "N-look" methods of speckle smoothing is to perform some type of digital processing technique in addition to or instead of N-look smoothing. Conventional imaging processing techniques have been developed for additive noise; however, if the log of the intensity is first obtained, then speckle noise becomes an additive noise [6] and conventional techniques can be applied [7].

In this paper a digital simulation of an image with speckle noise is developed and verified by comparison to experimentally obtained speckle imagery. The digital simulation is then used to obtain detection probability statistics and to evaluate various linear and nonlinear digital filtering techniques for speckle reduction.

II. SPECKLE THEORY

Radiation that has at least a partial degree of spatial and temporal coherence will exhibit speckle noise due to volume scattering while propagating through a medium such as the atmosphere or due to scattering from a rough surface. The physical origin of this noise is in the interference of many coherent wavelets that, because of the scattering, have traveled over different optical path lengths.

In free space propagation it is easy to see that many wavelets will contribute to the intensity at an observation point. In a perfect imaging system, diffraction causes the intensity at an image point to result from many wavelets.

To obtain speckle we require only that a large number of scattering events occur within the point spread function of the imaging system [1].

The electric field at any point (x,y) in our observation plane is, for a monochromatic wave

$$E = a(x,y)e^{i\omega t}$$

where $a(x,y)$ is the complex amplitude of the field. For both free space propagation and imaging, the amplitude is given by the sum of amplitudes of wavelets

$$a(x,y) = \sum_{k=1}^{N} |\alpha_k| \exp(i\phi_k) \quad . \tag{1}$$

To obtain the statistics of the electric field, we must solve the classical random walk problem [1,2]. In general, the statistics depend upon the coherence of the radiation and the statistics of the scattering surface or medium. For simplicity, we will assume that the radiation is coherent and linearly polarized. We will only consider speckle caused by scattering from a rough surface and will make those assumptions necessary to allow us to ignore the details of the scattering process [3]. The resulting statistics apply to speckle fields that were generated in this study.

The assumptions to be made are:

1. The scattering does not affect the polarization. To produce speckle in the laboratory, we rely upon multiple scattering in opal glass, which depolarizes the light. A polarizer is used in the recording of the speckle field to allow us to retain this assumption.

2. α_k and ϕ_k are statistically independent of each other and of all other α's and ϕ's. This assumption allows us to neglect the actual scattering event.

3. ϕ_k is uniformly distributed in the interval $-\pi$ to π. This assumption requires that the scattering surface be rough compared to a wavelength.

4. We will assume that the observation plane is in the far field. The statistics in the image plane are the same as the far field, provided there are a large number of independent scattering centers within the point spread function of the imaging system [1,2]. With these assumptions and for a value of N large enough to allow application of the central limit theorem, we can write speckle as a complex Gaussian field

$$a(x,y) = a_R(x,y) + i\, a_I(x,y) \tag{2}$$

where a_R, a_I are zero mean Gaussian random variables (for each x,y) with variance

$$\sigma_a^2 = E\left[a_R^2\right] = E\left[a_I^2\right] \quad . \tag{3}$$

The speckle intensity is then, simply

$$s = s(x,y) = a_R^2(x,y) + a_I^2(x,y) \tag{4a}$$

and phase

$$\theta = \theta(x,y) = \tan^{-1} \frac{a_I(x,y)}{a_R(x,y)} \tag{4b}$$

The random variables θ and s are found to be independent with densities

$$p(s) = \frac{1}{2\sigma_a^2} \exp\left(-s/2\sigma_a^2\right) \ , \ s \geq 0 \quad , \tag{5a}$$

$$p(\theta) = 1/2\pi, \ -\pi < \theta < \pi \quad , \tag{5b}$$

$$p(s,\theta) = p(s)\, p(\theta) \quad . \tag{5c}$$

The intensity at a point in the observation plane obeys negative exponential statistics and the phase obeys uniform statistics. Also the intensity and phase are statistically independent. We will call this fully-developed speckle.

The intensity is the parameter measured experimentally and thus of primary interest. The mean and variance of the intensity are given by

$$\mu_s \overset{\Delta}{=} E[s] = 2\sigma_a^2 \quad , \text{(mean)} \tag{6a}$$

$$m_{2,s} \triangleq E[s^2] = 2\mu_s^2 \quad , \text{(second moment)} \tag{6b}$$

$$\sigma_s^2 \triangleq E[(s-\mu_s)^2] = \mu_s^2 \quad , \text{(variance)} \tag{6c}$$

The contrast ratio (a measure of signal to noise) is defined as

$$C_r = \frac{\text{standard deviation}}{\text{mean}} \quad . \tag{7}$$

For fully developed speckle, $C_r = 1$ regardless of the signal strength. Thus, speckle is a signal dependent on multiplicative noise. This is in contrast to images with additive noise where a change in total light level can affect the apparent signal to noise [4].

A. Fully Developed Speckle in the Presence of Coherent Background (Ricean Statistics)

The effect of coherently adding a uniform intensity to the speckle intensity is of more than pedantic interest. If the assumption that the surface roughness is greater than a wavelength no longer can be made, then the resulting speckle pattern can be analyzed by assuming that it consists of a uniform field coherently added to a speckle field [1,2]. This would correspond to scattering from a slightly rough object with the uniform field corresponding to a specular reflection and the speckle field corresponding to diffuse scattering. We would expect to encounter this mixed beam case more often than the fully developed case (for example, holography).

In this case the speckle complex amplitude contains a constant phasor so that

$$a = a_S + a_R + j\, a_I \quad , \tag{8}$$

a_S = constant with a fixed phase angle (zero phase angle can be assumed).

Let $a_s^2 = s_o$. Then

$$\hat{s} = (a_S + a_R)^2 + a_I^2$$

$$= s_o + s + 2a_S a_R \quad . \tag{9}$$

The statistics of $\hat{s}$ are given as follows:

Joint Density

$$p(\hat{s},\theta) = \begin{cases} \frac{1}{4\pi\sigma^2} \exp\left(-\frac{\hat{s} + s_o - 2\sqrt{\hat{s}\, s_o}\cos\theta}{2\sigma_a^2}\right), & s \geq 0,\ -\pi \leq \theta \leq \pi \\ 0\ , \text{ otherwise.} \end{cases} \tag{10}$$

Marginal Density

$$p(\hat{s}) = \begin{cases} \frac{1}{\mu_s} \exp\left(-\frac{\hat{s} + s_o}{\mu_s}\right) I_o\left(2\sqrt{s\ \hat{s}_o}/\mu_s\right), & s \geq 0 \\ 0\ , \text{ otherwise.} \end{cases} \tag{11}$$

$I_o(.)$ = zero order modified Bessel function of first kind.

Mean

$$\begin{aligned} \mu_{\hat{s}} = E[\hat{s}] &= E[s] + s_o + 2E\ [a_s a_R] \\ &= E[s] + s_o + 2E\ [a_s]\ E\ [a_R] \\ &= E[s] + s_o = \mu_s + s_o \quad . \end{aligned} \tag{12}$$

Second Moment

$$E\ [(\hat{s})^2] = 2\mu_s^2 + 4\mu_s s_o + s_o^2 \quad . \tag{13}$$

Variance

$$\sigma_{\hat{s}}^2 = \mu_s^2(1 + 2r), \text{ where } r = \text{beam ratio} = s_o/\mu_s \tag{14}$$

The contrast ratio is given by

$$C_r = \sqrt{1 + 2r}/(1 + r) \quad . \tag{15}$$

For large values of r

$$C_r \cong \sqrt{2/r} \tag{16}$$

B. N-Look Averaging

One method used to reduce speckle noise is the intensity addition of N speckle patterns

$$s = \sum_{k=1}^{N} s_k \quad . \tag{17}$$

If each speckle field s_k is statistically independent of all the other N-1 fields, and all the average intensities μ_k are distinct, i.e., $\mu_k \neq \mu_\ell$ if $k \neq \ell$, then the probability density is

$$p(s) = \sum_{k=1}^{N} \frac{\mu_k^{N-2}}{\prod_{\substack{p=1 \\ p\neq k}}^{N} (\mu_k - \mu_p)\ \delta_{k,p}} \exp\left(-\frac{s}{\mu_k}\right), \quad s \geq 0 \tag{18}$$

$$p(s) = 0, \text{ otherwise.}$$

If the average intensity is the same for all N fields [1], i.e., $\mu_k = \mu_o$ for $k = 1,\ldots,N$, then

$$p(s) = \frac{s^{N-1}}{(N-1)!\ \mu_o^N} \exp\left(-\frac{s}{\mu_o}\right), \quad s \geq 0$$

$$= 0, \quad s \geq 0 \quad . \tag{19}$$

The average value of intensity, the variance and the contrast ratio may be calculated from this probability density function giving

$$\langle s \rangle = \mu_o \tag{20}$$

$$\langle s^2 \rangle = (1 + 1/N)\ \mu_o^2 \tag{21}$$

$$\sigma^2 = \mu_o^2/N \tag{22}$$

$$\gamma = 1/\sqrt{N}\ . \tag{23}$$

III. DIGITAL MODEL

For our initial experiments, a very simple test pattern was selected. This test pattern consists of a 64 x 192 array of pixels which contain square cells of sizes 1 x 1, 2 x 2, 4 x 4, 8 x 8, and 16 x 16 at eight different intensities. This pattern is similar to a chart developed by Rose[8] for experiments in human vision. This type of pattern was also used in a previous investigation of speckle noise[9]. Figure 1 shows the optical and digital test patterns

If we let

$v(x,y)$ = image intensity at x,y

$T(x,y)$ = object transmittance (or reflectivity) at x,y

then

$$v(x,y) = T(x,y)\, s(x,y) \tag{24}$$

is the speckle image model in the simplest case with no receiver noise.

To generate the speckle noise intensity $s(x,y)$ for fully developed speckle, we first generate a pseudo-random pair of Gaussian random variables, then calculate their magnitude squared. This algorithm, repeated for every point in the image field, will produce a speckle noise field. One hundred twenty eight speckle noise fields 64 x 192 pixels in size were digitally generated.

In addition to the noise fields with fully developed speckle, eight frames of size 64 x 192 that contain speckle noise with Ricean statistics were generated. The beam ratios selected were 0, 2.41, 6.46, 14.48, 30.49, 62.5, 126.5 and 254.5. These beam ratios were selected to provide the same beam ratio C_r as occurs in N-look averaging for N=1, 2, 4, ..., 128.

In the more general case of spatially invariant diffraction limited imaging geometry, the observed image is given by first finding the amplitude field in the imaging plane as

$$A(x,y) = \int_{-\infty}^{\infty} \int_{-\infty}^{\infty} K(x-\zeta,\, y-\eta)\, \alpha(\zeta,\eta)\, d\zeta\, d\eta \tag{25}$$

where $\alpha(\zeta,\eta)$ is the complex amplitude distribution of the object. Then the image intensity is given by

$$v(x,y) = \left| A(x,y) \right|^2 + n(x,y) \tag{26}$$

where $n(x,y)$ represents the additive detector noise.

IV. MODEL VALIDATION: N-LOOK FILTER RESULTS

Figure 2 shows the histogram of the digital test pattern in the presence of fully developed speckle. This histogram represents the convolution of the test pattern intensity distribution with the speckle intensity distribution given by (5a). Figure 3 shows the histogram of the Ricean speckled test pattern for $\gamma = 6.46$ (Note that $\gamma = 0$ would be the same as fully developed speckle).

To validate the digital speckle models we compare the N-look, linear temporal averaging filter outputs of digital and optical experiments. Let

$$v_k(x,y) = T(x,y)\, s_k(x,y) \tag{27}$$

where $k = 1, \ldots, N$ and v_k represents the k^{th} image of the object. Then

$$E[v_k] = TE[s_k] - T\mu_s \quad . \tag{28}$$

This suggests

$$T_N(x,y) = \frac{1}{\mu_s} \frac{1}{N} \sum_{k=1}^{N} v_k(x,y) \tag{29}$$

as an estimate of $T(x,y)$. This is a point by point (i.e., for each x,y) average of N independent samples of a random variable. Therefore,

$$E[\hat{T}_N] = \frac{1}{\mu_s^2} \left\{ \frac{1}{N} \sum_{k=1}^{N} E[v_k] \right\} = T \tag{30}$$

which means $\hat{T}_N$ is an unbiased estimate of T. Using a probability model such as (19) for $\hat{T}_N$, it is quite easy to show that it is the maximum likelihood estimate of T given $v_k(x,y)$, $k=1,\ldots,N$. Also,

$$E[T_N^2] = \frac{1}{\mu_s^2} \cdot \frac{T^2}{N^2} \sum_{k,\ell=1}^{N} E[s_k s_\ell] \quad . \tag{31}$$

Since s_k and s_ℓ are independent from (6b) we get

$$E[s_k s_\ell] = \begin{cases} 2\mu_s^2 & k = \ell \\ \mu_s^2 & k \neq \ell \quad . \end{cases} \tag{32}$$

This gives

$$E[\hat{T}_N^2] = \frac{T^2}{N} + T^2 \quad . \tag{33}$$

From (33) we have

$$\text{var}[\hat{T}_N] = E[\hat{T}_N - E(\hat{T}_N)]^2 = \frac{T^2}{N} \quad . \tag{34}$$

Therefore the contrast ratio is

$$\gamma = \frac{T}{\sqrt{N}} \cdot \frac{1}{T} = \frac{1}{\sqrt{N}} \quad . \tag{35}$$

Thus the contrast should improve by $\sqrt{N}$ as the number of looks, N is increased.

The above N look digital filter was applied to a sequence of 128 computer simulated speckle images of the digital test pattern of Figure 1. Filtered outputs for N=1,2,4,8,16,32,64 and 128 were produced (see Figure 4). Output images were displayed on a high quality TV monitor and photographs were made for evaluation by a set of observers. The observers made independent evaluations of the minimum detectable contrast as a function of the object size for the digital imagery and for optical images produced (see Figure 5 [4] using the test pattern in Figure 1). Figure 6 [10] shows the comparison between the optical and digital speckle experiments for minimum detectable contrast for objects whose size (area) is about sixteen times the speckle size. The results show agreement between the two experiments except for the effects due to the optical transfer function. The reader can perform his own evaluation by comparing the digitally produced data shown in Figure 4 with the optically produced data in Figure 5. The effect of the optical transfer function can be seen in the N-128 case in Figure 5 where the low contrast elements of rows 3 and 4 are not visible. To verify the Ricean speckle model, one needs to compare the digital and optical Ricean speckle images at various beam ratios. It has been established earlier[4] that a Ricean speckle with beam ratio r and an N-look temporarily averaged speckle have the same contrast when

$$\frac{\sqrt{1 + 2r}}{1 + r} = \frac{1}{\sqrt{N}}$$

$$\text{or } r = N + \sqrt{N^2 - N} - 1 \quad . \tag{36}$$

Thus Ricean speckle at r = 0, 2.41, 6.46, 14.48, 30.49, 62.5, 126.5 and 254.5 corresponds to the N-look averaged speckle for N = 1,2,4,8,16,32,64 and 128 respectively. Figure 7[10] shows the digitally and optically produced Ricean speckle images respectively. An agreement consistent with Figure 6 was obtained in this case also.

The agreement obtained between the optical and digital imagery validates the use of the digital model in speckle noise experiments involving human observers.

Nonlinear Temporal Filters

It is difficult to accomplish nonlinear filtering of speckle noise in an optical system. However, in a digital system it is quite easy to produce nonlinear filters. Two nonlinear filters that were simple to implement digitally were selected for the initial experiments.

Square Root Filter

From Eq. (27) we can write

$$v_k^{1/2} = T^{1/2}\, s_k^{1/2} \tag{37}$$

or

$$T^{1/2} = E[v_k^{1/2}]/E[s_k^{1/2}] \tag{38}$$

which suggests

$$\hat{T}_N(x,y) = \left\{ \frac{1}{N} \sum_{k=1}^{N} v_k^{1/2}(x,y)/E[s_k^{1/2}] \right\}^2$$

$$= \frac{16}{\mu_s \pi} \left[\frac{1}{N} \sum_{k=1}^{N} v_k^{1/2}(x,y) \right]^2 . \tag{39}$$

Squaring Filter

Also from Eq. (27)

$$v_k^2 = T^2\, s_k^2 \tag{40}$$

which gives

$$T = \left\{ E[v_k^2]/E[s_k^2] \right\}^{1/2} \tag{41}$$

and

$$N_N = \frac{1}{\sqrt{2}\,\mu_s} \left(\frac{1}{N} \sum_{k=1}^{N} v_k^2 \right)^{1/2} \tag{42}$$

as another estimate of T.

These nonlinear filters did not produce a measurable change in the minimum detectable contrast compared to the linear temporal filter. Observers did comment however that the noise in the squaring filter data appeared less objectionable. Experimental results using these filters are shown together with spatial averaging results of the next section.

V. SPATIAL FILTERS FOR SPECKLE REDUCTION

The results of the N-look temporal averaging method show that a large number of looks ($N > 8$) may be required to detect objects which have small size and/or low contrast. Spatial filtering of speckle images offers a means of speckle noise reduction when the number of available looks is not very large. We consider several simple linear spatial filters.

A. Spatial Averaging Filter

A standard technique used to reduce speckle noise in synthetic aperture radar systems is to integrate the intensity values of adjacent pixels. This type of speckle filtering is digitally produced very easily in the following fashion. Let

$$\hat{v}_N(x,y) \triangleq \frac{1}{N} \sum_{k=1}^{N} v_k(x,y) \tag{43}$$

and define a spatial average v_N as

$$\begin{aligned} \bar{v}_N(x,y) = {}& \tfrac{1}{2}[v_N(x,y) + \tfrac{1}{4}\{v_N(x - \Delta,y) \\ & + v_N(x + \Delta,y) + v_N(x,y - \Delta) \\ & + v_N(x,y + \Delta)\}] \quad . \end{aligned} \tag{44}$$

For digital images x,y are integer indices and $\Delta = 1$. From Eqs. (27) and (43) we would have

$$\hat{T}_N(x,y) = \frac{1}{\mu_s} \bar{v}_N(x,y) \tag{45}$$

if T(x,y) is almost constant over the averaging window. In general, the size of the window will govern the tradeoff between resolution and speckle noise suppression. In these experiments, the spatial filter improved object recognition for the larger objects with an accompanying reduction in resolution. The spatial filter was combined with each of the other filters (linear, square, and square root) and the results are shown in Figure 8. The minimum detectable contrast of large objects for a linear temporal averaging of N with spatial averaging is approximately equal to the same minimum detectable contrast for a linear temporal averaging of 2N without spatial averaging. Figure 8 shows that, as was the case without spatial filtering, the nonlinear filters produce no visible improvement.

3. Homomorphic Filtering for Speckle Reduction

Since speckled images involve multiplicative noise, linear filtering methods may not be employed arbitrarily. Consider an N-look averaged speckle image given as

$$\hat{V}_N(x,y) = T(x,y)\ \hat{S}_N(x,y)\ ,\ T \geq 0\ ,\ \hat{S} \geq 0 \tag{46}$$

where $\hat{S}_N(x,y)$ represents the speckle noise after averaging over N looks. Taking the logarithm of both sides of (46) we can write

$$W_N(x,y) = Z(x,y) + \eta_N(x,y) \tag{47}$$

where

$$W_N(x,y) = \log \hat{V}_N(x,y)$$

$$Z(x,y) = \log T(x,y)$$

$$\eta_N(x,y) = \log \hat{S}_N(x,y)$$

Eq. (47) now represents observations $W_N(x,y)$ of a signal $Z(x,y)$ in the presence of additive noise $\eta(x,y)$. It has been shown by Arsenault[11] that for $N \geq 2$, the additive noise may be modeled reasonably well by a Gaussian density function. Regardless of the probability distribution of η_N, one can design easily optimum linear filters to estimate $Z(x,y)$ from $W_N(x,y)$. Figure 9 shows the block diagram of the overall filter algorithm. This filter is also called a homomorphic filter. We shall compare this filter with the conventional filtering method shown in Figure 10. Here, we use the same filter as in homomorphic filtering, but logarithmic and exponential operations are deleted. The following filters are considered.

C. Low Pass Filter (F1)

An ad-hoc digital low pass filter was designed to filter the noise. The frequency response of this filter is given by

$$H(\omega_x,\ \omega_y) = h(\omega_x)\ h(\omega_y) \tag{48}$$

where ω_x and ω_y are the spatial frequency variables in the Fourier transform domain of the sampled images. Figure 11 shows the normalized frequency response $h(\omega)$. The passband is chosen to be $\left[-\frac{\pi}{4}\ ,\ \frac{\pi}{4}\right]$ and the transition width to be $\frac{\pi}{64}$. The filter was implemented via the discrete Fourier transformation of the speckle image.

D. Wiener Filter (F2)

For a signal with additive noise, the frequency response of the optimum linear mean square filter (called the Wiener filter) is given by

$$G(\omega_x, \omega_y) = S_Z(\omega_x, \omega_y)/(S_Z(\omega_x, \omega_y) + S_\eta(\omega_x, \omega_y)) \tag{49}$$

where S_Z and S_η denote the spectral density functions of the signal and noise processes. Since in our digital simulations the speckle size was chosen to coincide with the sampling grid size, the fully developed speckle field is independent from pixel to pixel. Hence, $\eta_N(x,y)$ can be considered as a white noise field of mean μ_η and μ_Z, the mean value of Z to be zero by subtracting the sample mean μ_W of the observation field from each observation $W_N(x,y)$. Hence, for zero mean data

$$S_\eta(\omega_x, \omega_y) = \sigma_\eta^2 = \begin{cases} \frac{\pi^2}{6} & , N = 1 \\ \\ \frac{1}{N} & , N \geq 2 \end{cases} \tag{50}$$

where we have used the result of Arsenault[11] to evaluate σ_η^2. To estimate the spectral density of the signal $Z(x,y)$ we assume its covariance function is exponentially decreasing in each dimension, i.e.,

$$\begin{aligned} \text{Cov}[Z(x,y)] &= E[(Z(x',y') - \mu_Z)(Z(x+x',y+y') - \mu_Z] \\ &= \sigma_Z^2 \, \rho_x^{|x|} \, \rho_y^{|y|} \end{aligned} \tag{51}$$

where $0 \leq |\rho| \leq 1$. For zero mean observation $W_N(x,y)$, the parameters ρ_x, ρ_y can be estimated as

$$\rho_x \simeq \sum_x \sum_y W(x,y)\, W(x+1,y) / \left(\sum_x \sum_y (W(x,y))^2\right) \tag{52a}$$

$$\rho_y \simeq \sum_x \sum_y W(x,y)\, W(x,y+1) / \left(\sum_x \sum_y (W(x,y))^2\right) \tag{52b}$$

The variance σ_Z^2 is estimated from σ_W^2 the sample variance of $W(x,y)$ as

$$\sigma_Z^2 = \sigma_W^2 - \sigma_\eta^2 \quad .$$

Note that this model does not require the a priori knowledge of the object covariance since all the measurements are made on the available data. Experimentally, this model was found to be satisfactory although a better covariance model would be ultimately desirable. The object spectral density function corresponding to the foregoing covariance model is simply given by its Fourier transform as

$$S_Z(\omega_x, \omega_y) = \beta^2 \, [(1 - 2\alpha_x \cos\omega_x \, ((1 - 2\alpha_y \cos\omega_y)]^{-1} \tag{53}$$

where

$$\beta^2 = \sigma_Z^2 (1 - \rho_x^2)(1 - \rho_y^2)/(1 + \rho_x^2)(1 + \rho_y^2)$$

$$\alpha_x = \rho_x/(1 + \rho_x^2) \ , \ \alpha_y = \rho_y/(1 + \rho_y^2)$$

Given S_Z and S_y, the Wiener filter design is complete. It is implemented via the discrete Fourier transform of the sampled image as follows:

1. Take the logarithm of the image $\hat{V}_N(x,y)$ to obtain $W_N(x,y)$.

2. Find the sample mean of $W_N(x,y)$ and subtract from each pixel value.

3. Calculate ρ_x, ρ_y, σ_Z^2 and the Wiener filter frequency response.

4. Take the discrete Fourier transform (DFT) of the image (of appropriate size). In the present case (see examples in paragraph G below) a 256x256 transform was adequate.

5. Multiply the image DFT with the Wiener filter gain sampled at appropriate frequencies.

6. Take inverse DFT, exponentiate and scale the image appropriately for display.

E. Spatial Averaging Filter (F3)

The homomorphic spatial filter is implemented by spatial averaging of $W_N(x,y)$ according to (44).

F. Median Filter (F4)

Here a spatial window of suitable size (3x3 here) is chosen. We slide this window on the image field $W_N(x,y)$ and for each position, replace the pixel value at the center of the window by the median value of all the pixels lying in the window.

G. Examples and Comparisons

The foregoing filters (F1 to F4) were implemented digitally both in the homomorphic mode and in the conventional mode. In the homomorphic mode, the logarithmically transformed image is the input to a spatial filter and its output is exponentiated (Fig 9). In the conventional mode, the logarithmic and the exponential transformation are deleted. The spatial filters, once designed, are kept the same in either mode.

Figure 12 shows the test pattern used and the corresponding N-look averaged speckle images for N=1,2,4 that are available for digital processing. Figures 13 to 16 show the results of applying homomorphic filters F1 to F4 to these images. These results show that filters F1, F2 and F3 tend to smooth the speckle. The median filter performs some smoothing but distorts smaller

objects. In a detection experiment this could cause high false alarm rates. This is not completely surprising because the median filter is known to perform well on binary noise whereas presently (in the homomorphic mode) the noise is nearly Gaussian.

Figures 17 to 19 compare the performances of the various homomorphic filters. Since the noise is additive and nearly Gaussian as expected, we find the Wiener filter to give the best performance. The low pass filter tends to oversmooth and somewhat distort the size and shape of the objects. The median filter affects most, the resolution of objects to which are close to the size of the median filter window. It is notable that both the Wiener and Spatial averaging filters are able to resolve objects of smaller size (see the fourth and the fifth rows).

Finally, we compare the conventional vs homomorphic filters in Figures 20 to 23. For larger objects (low resolution), the performance of the linear and homomorphic filters is nearly equivalent. However for smaller size objects (rows 3, 4, and 5) i.e., at higher resolution, the homomorphic filters definitely seem to perform better. This is particularly noticeable for the Wiener and Spatial averaging filters (Figures 21, 22).

H. Conclusion

Based on the foregoing experiments we conclude the following:

1. Homomorphic filtering has a definite advantage over straightforward linear filtering for speckle reduction.

2. The homomorphic Wiener filter yields most favorable results in terms of resolution vs noise reduction. More accurate object spectral density models could be useful in the design of Wiener filters.

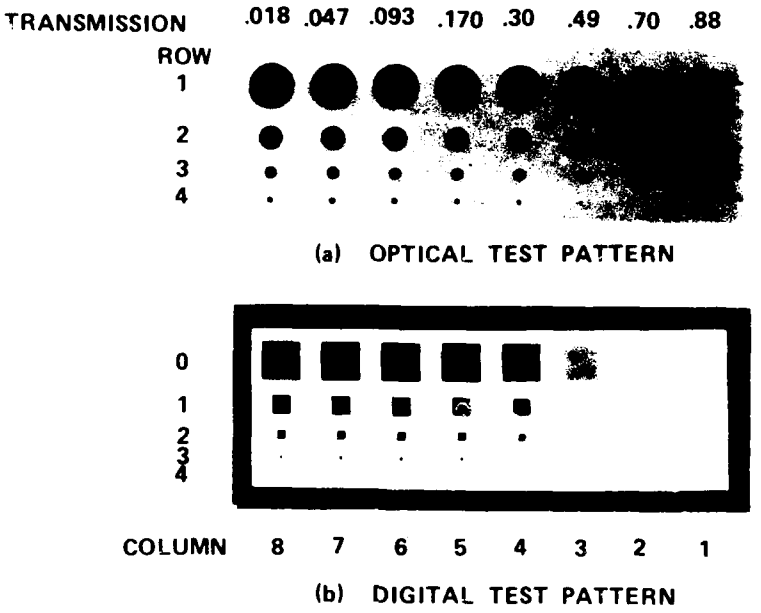

Figure 1. Optical and digital test patterns.

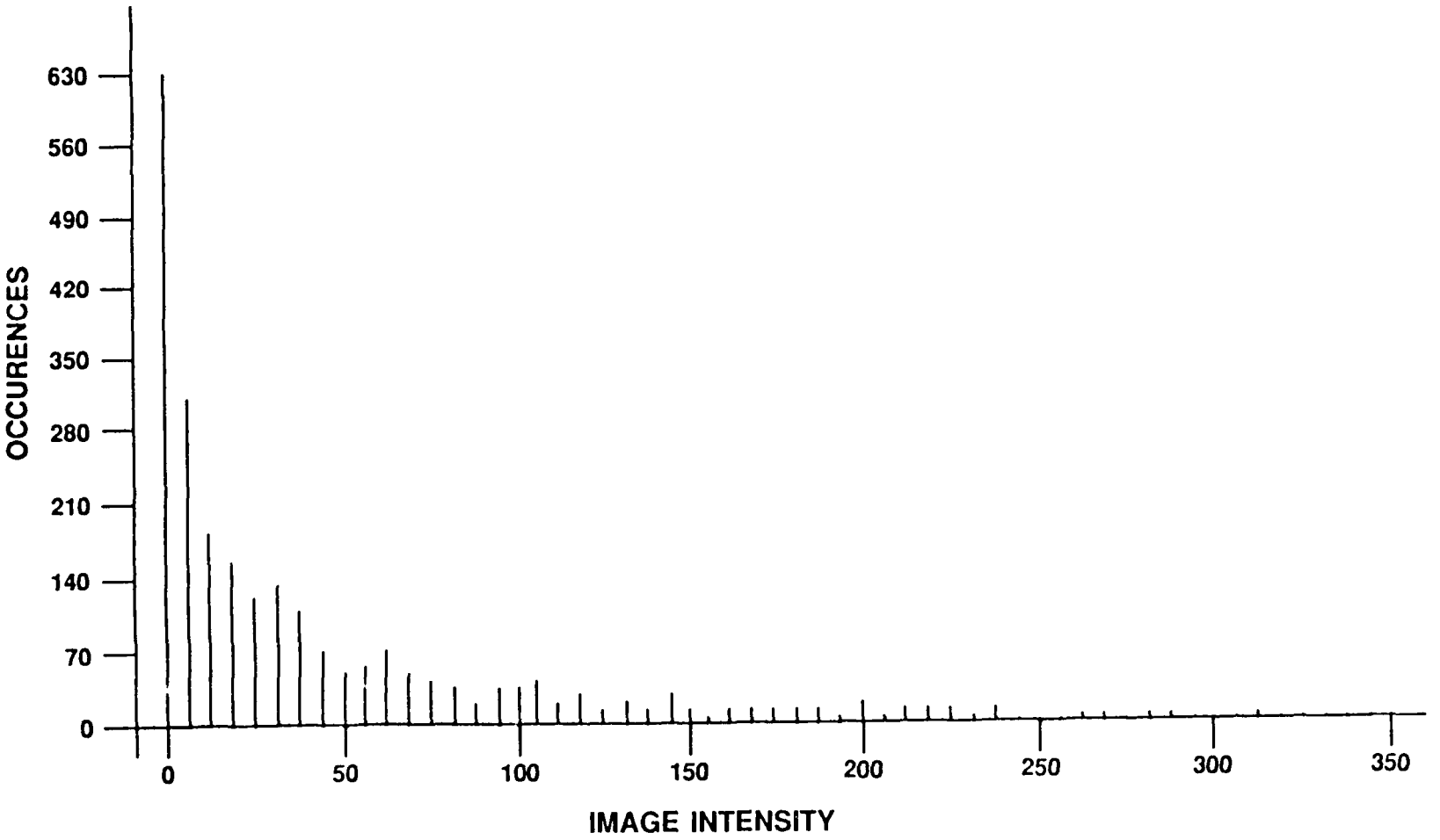

Figure 2. Histogram of the digital test pattern with fully developed speckle noise.

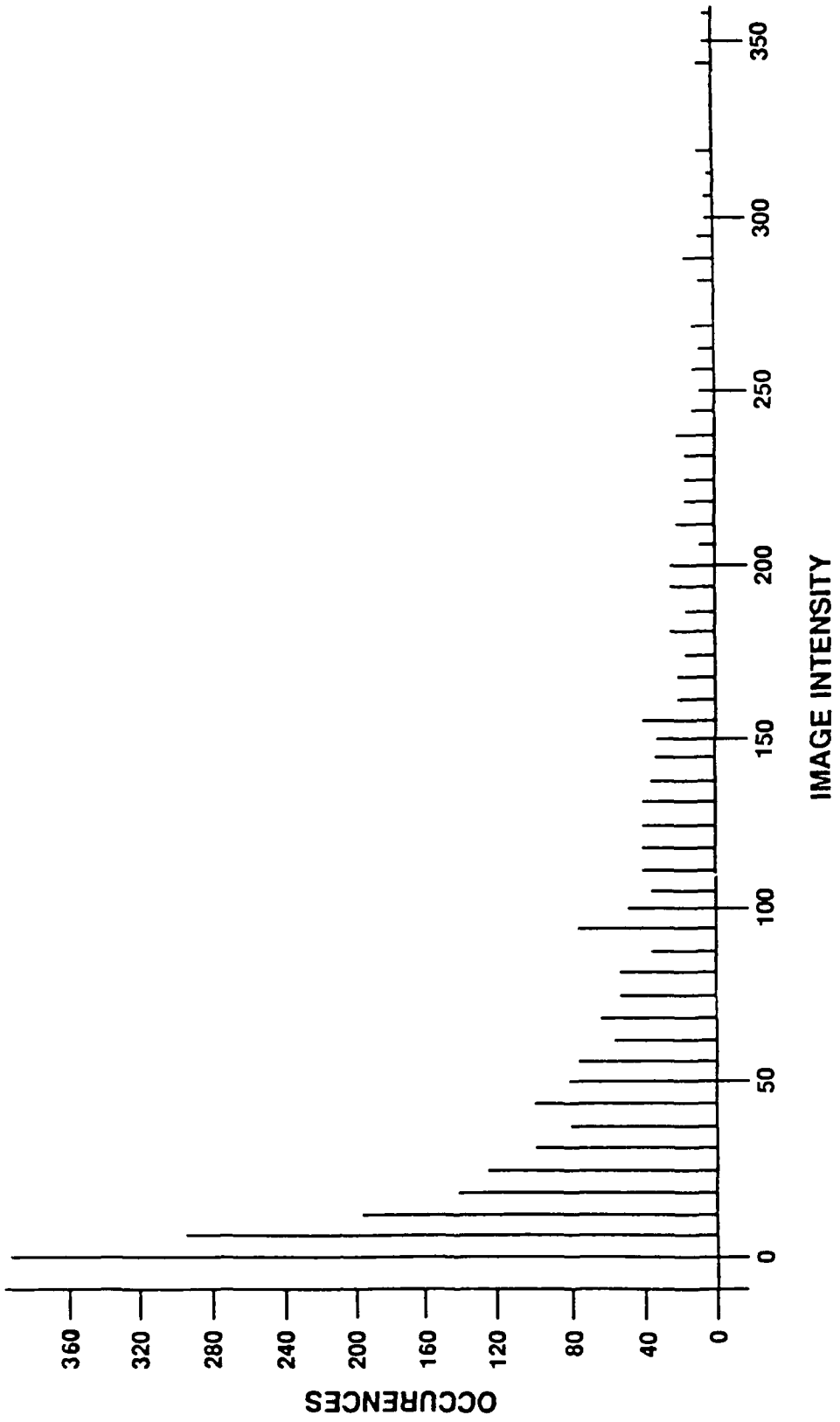

Figure 3. Histogram of the digital test pattern with Ricean speckle noise, $\gamma = 6.46$.

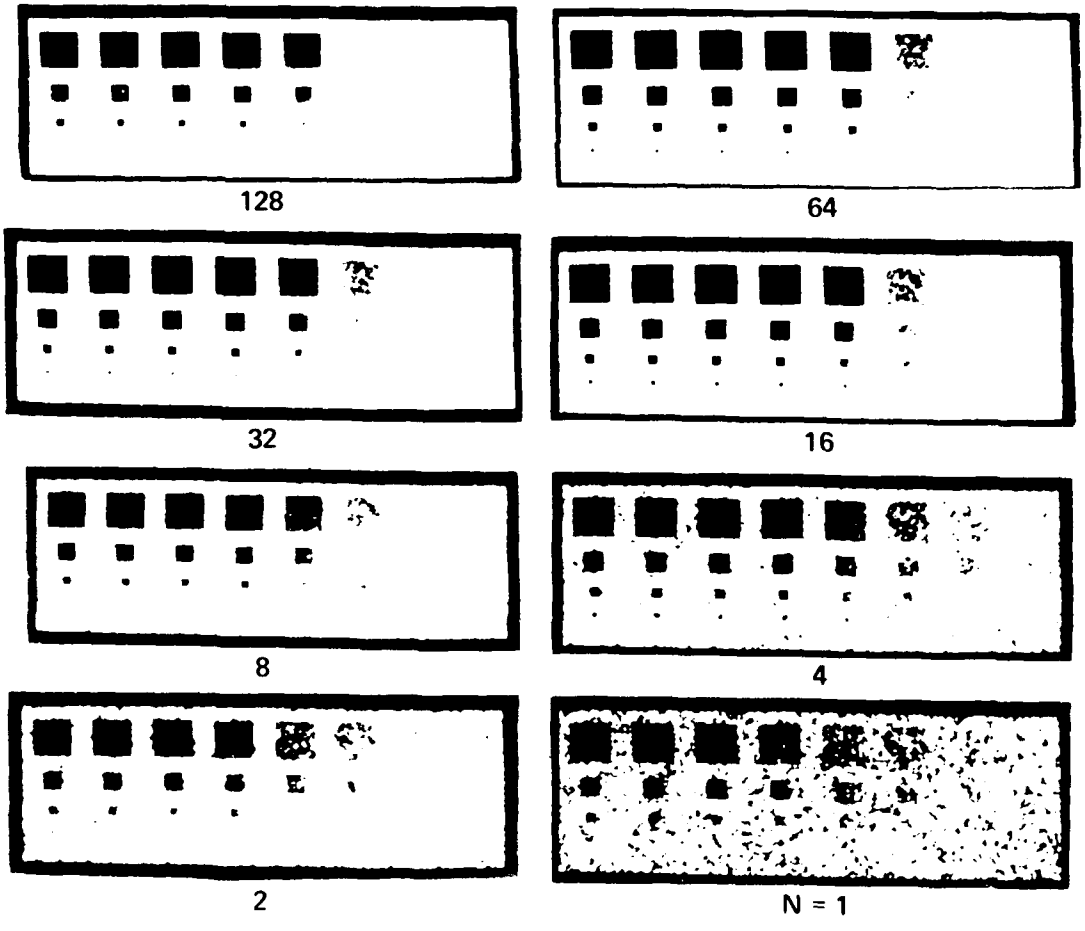

Figure 4. Digital N-look averaging of speckle.

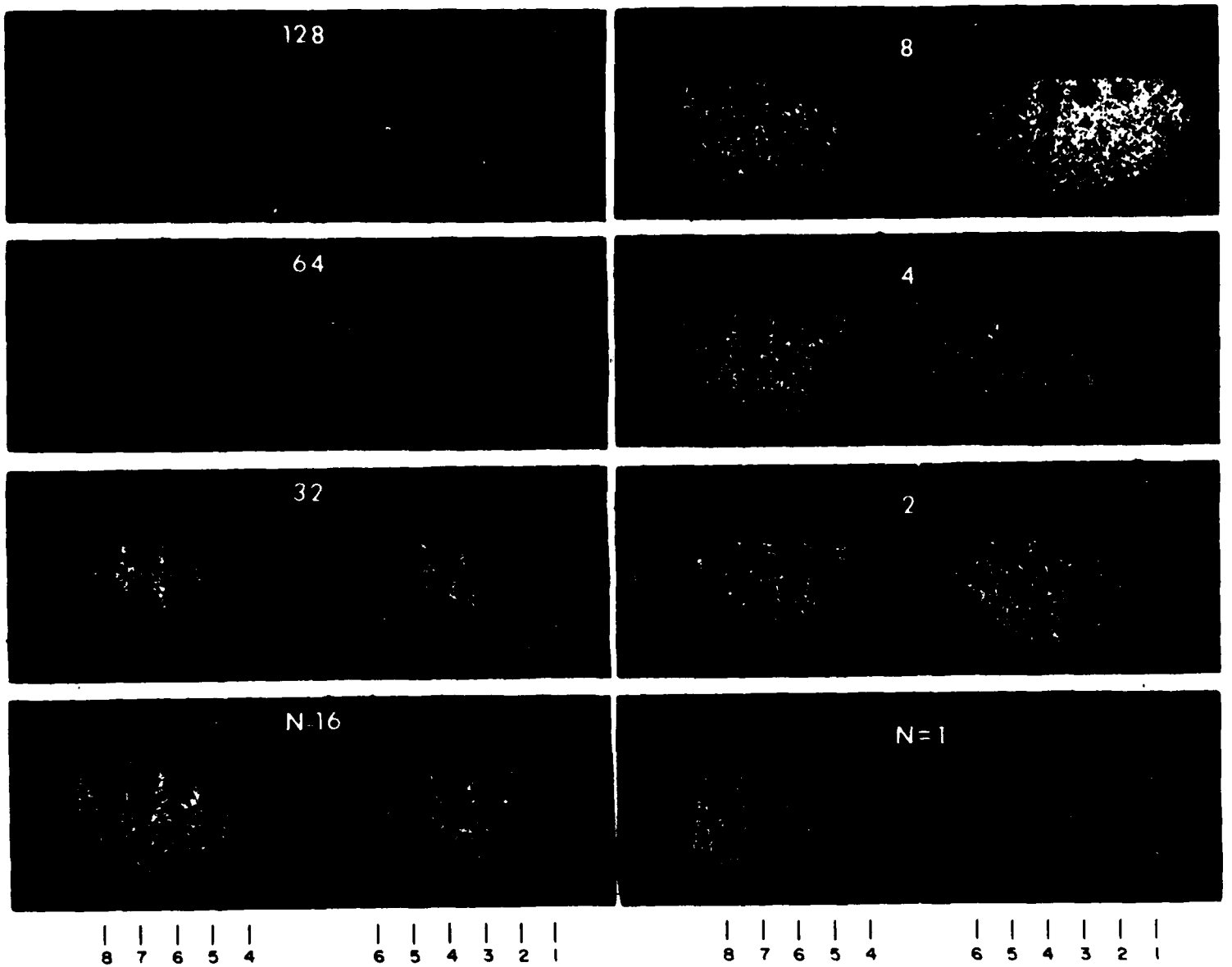

Figure 5. Optical N-look averaging of speckle. [4]

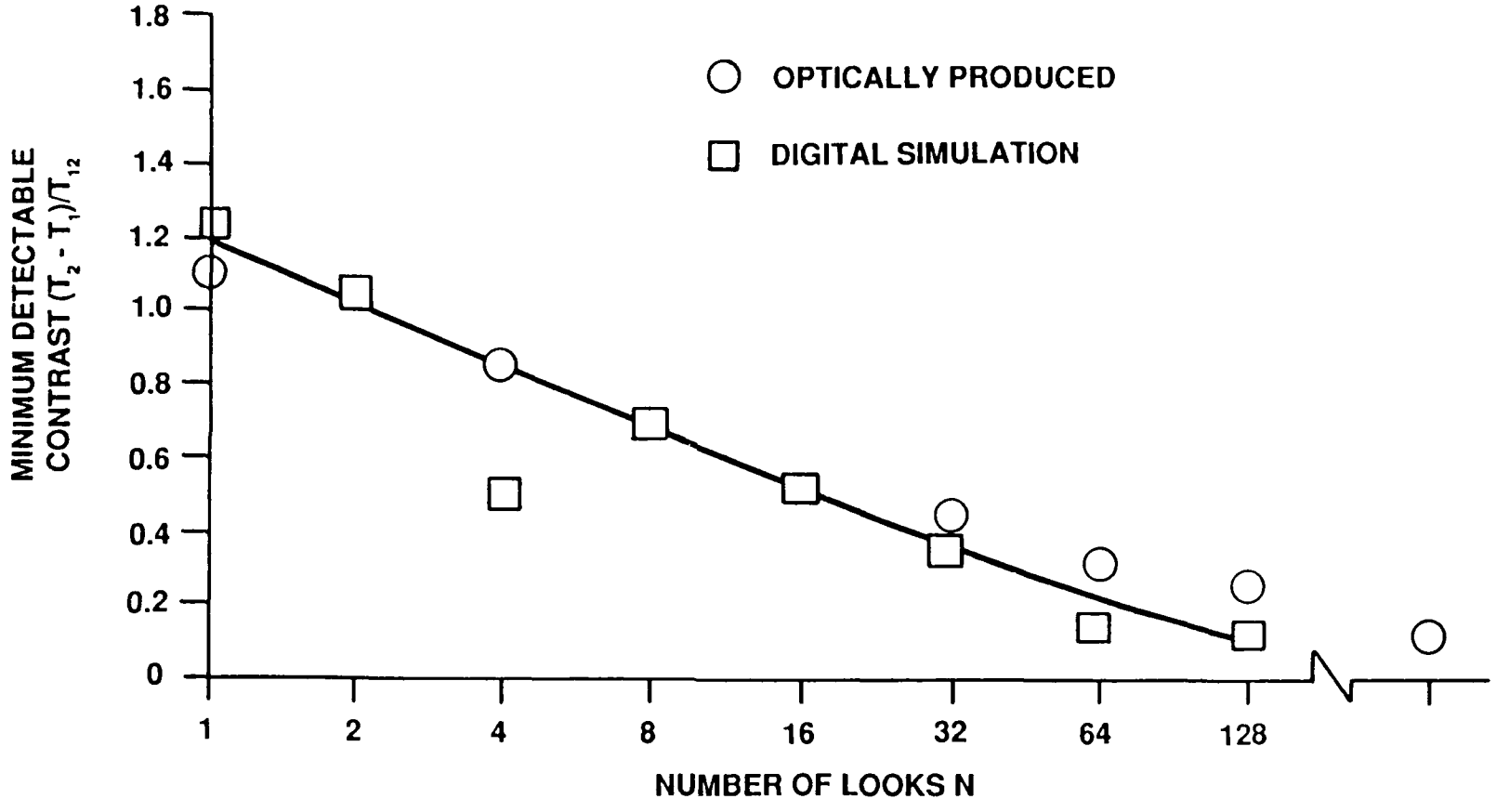

Figure 6. Contrast required to detect objects sixteen times the speckle size. [10]

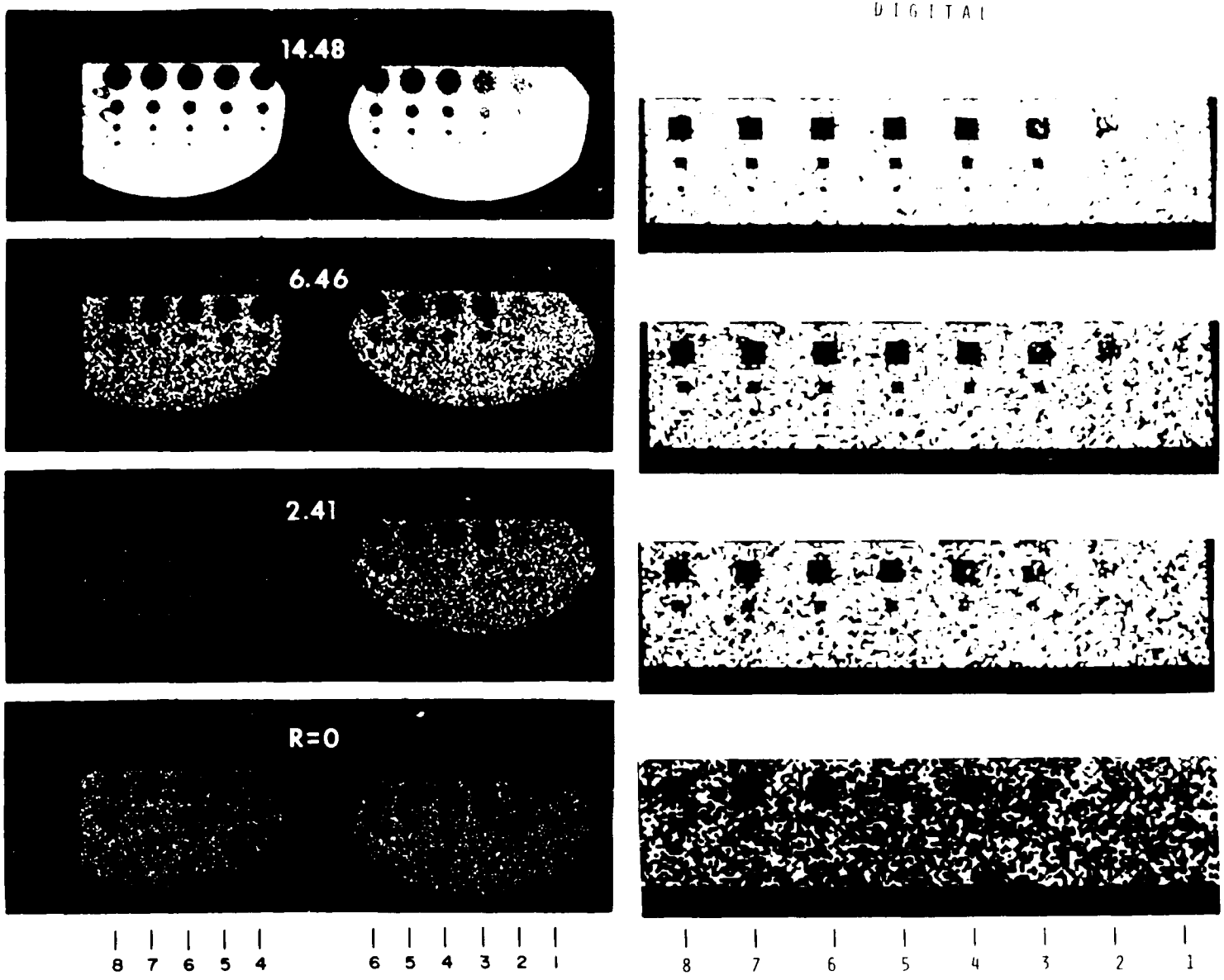

Figure 7. Optical and digital simulations of Ricean speckle images. (Page 1 of 2)

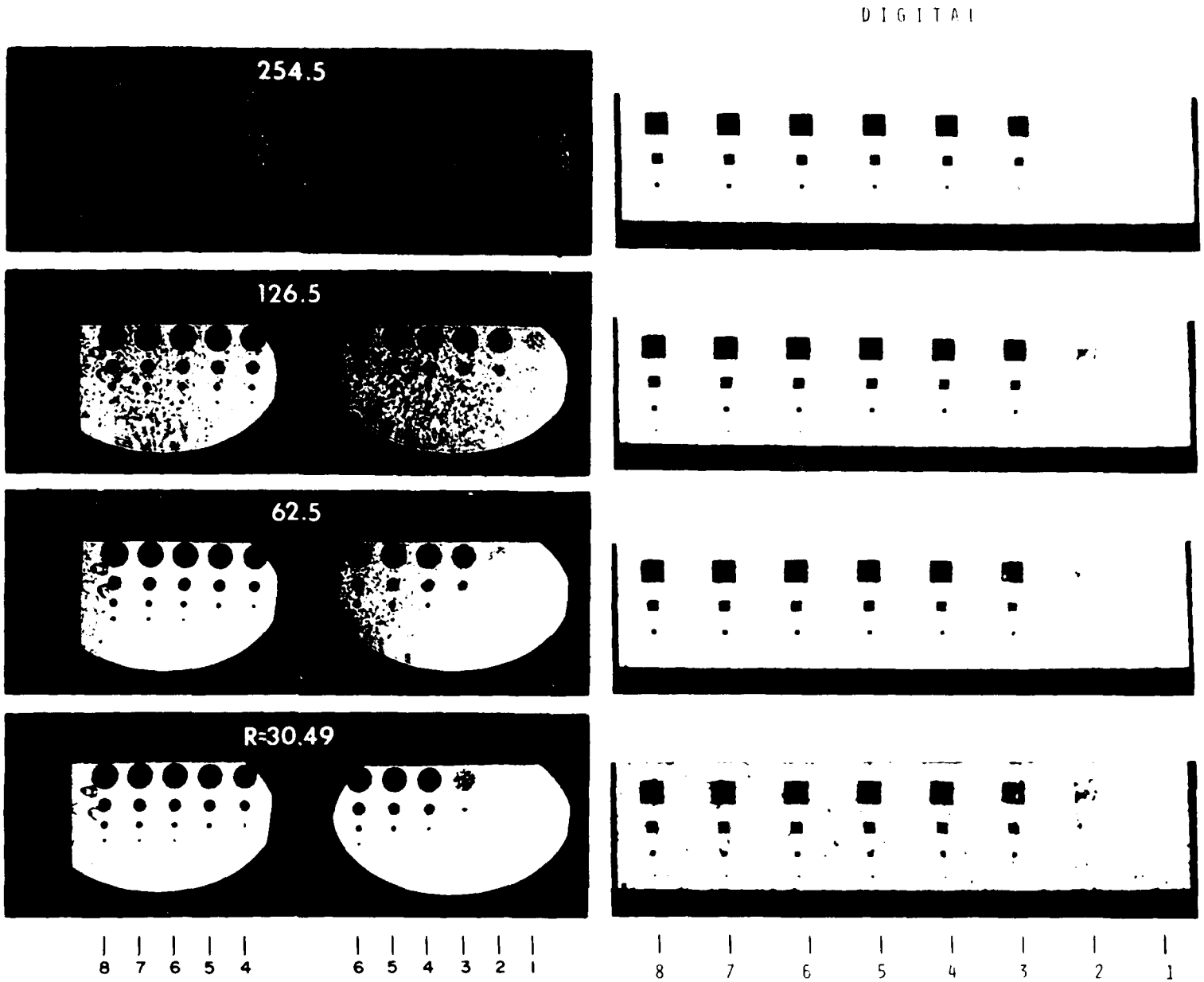

Figure 7. Optical and digital simulations of Ricean speckle images. (Page 2 of 2)

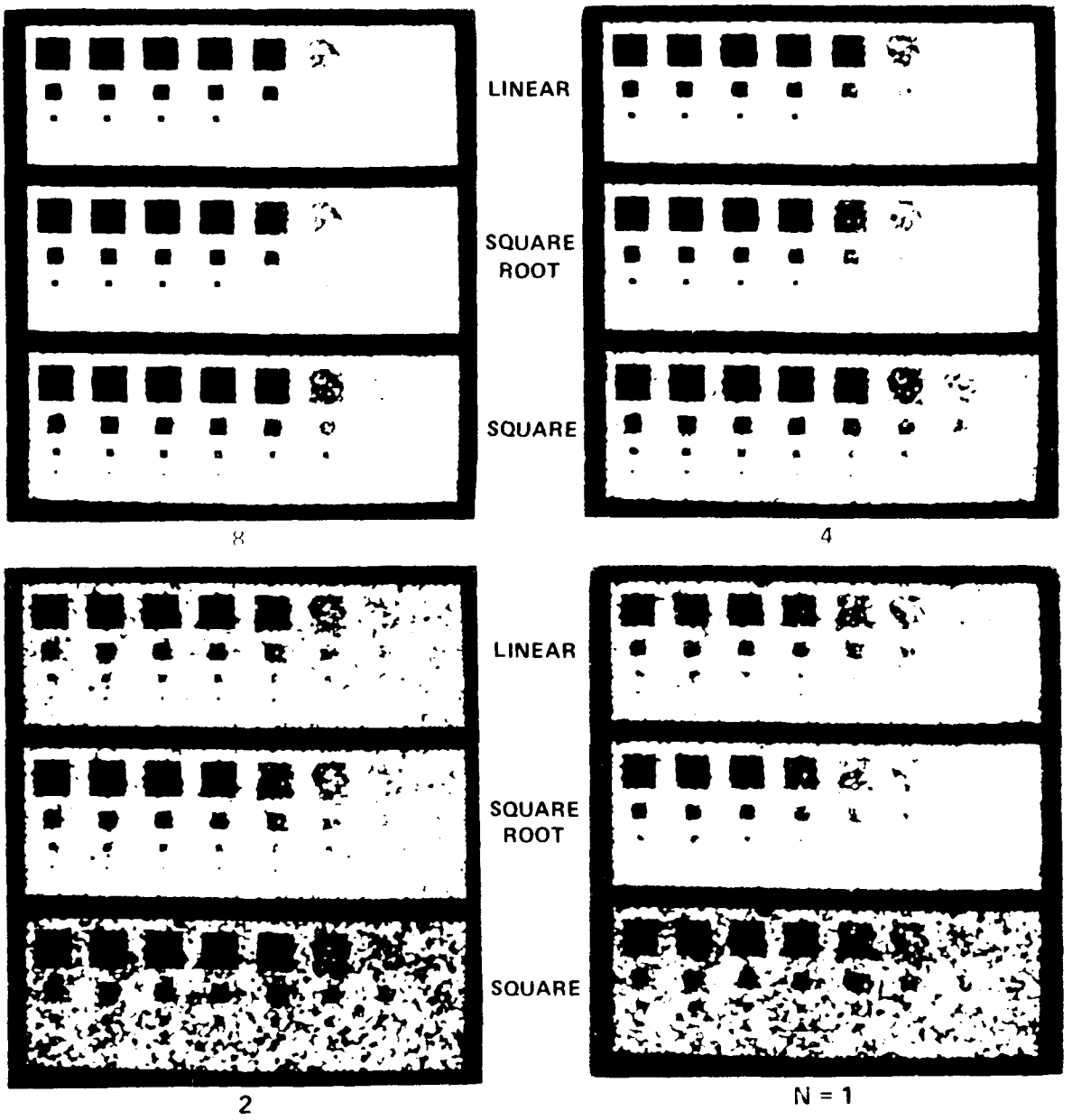

Figure 8. Spatial averaging applied to three types of filters.

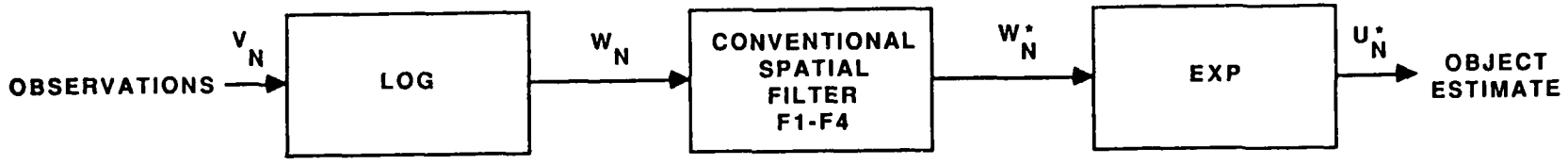

Figure 9. Homomorphic filtering.

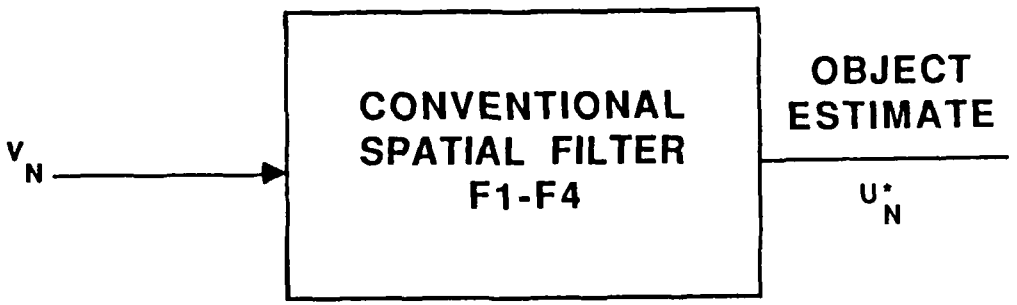

Figure 10. Conventional filtering.

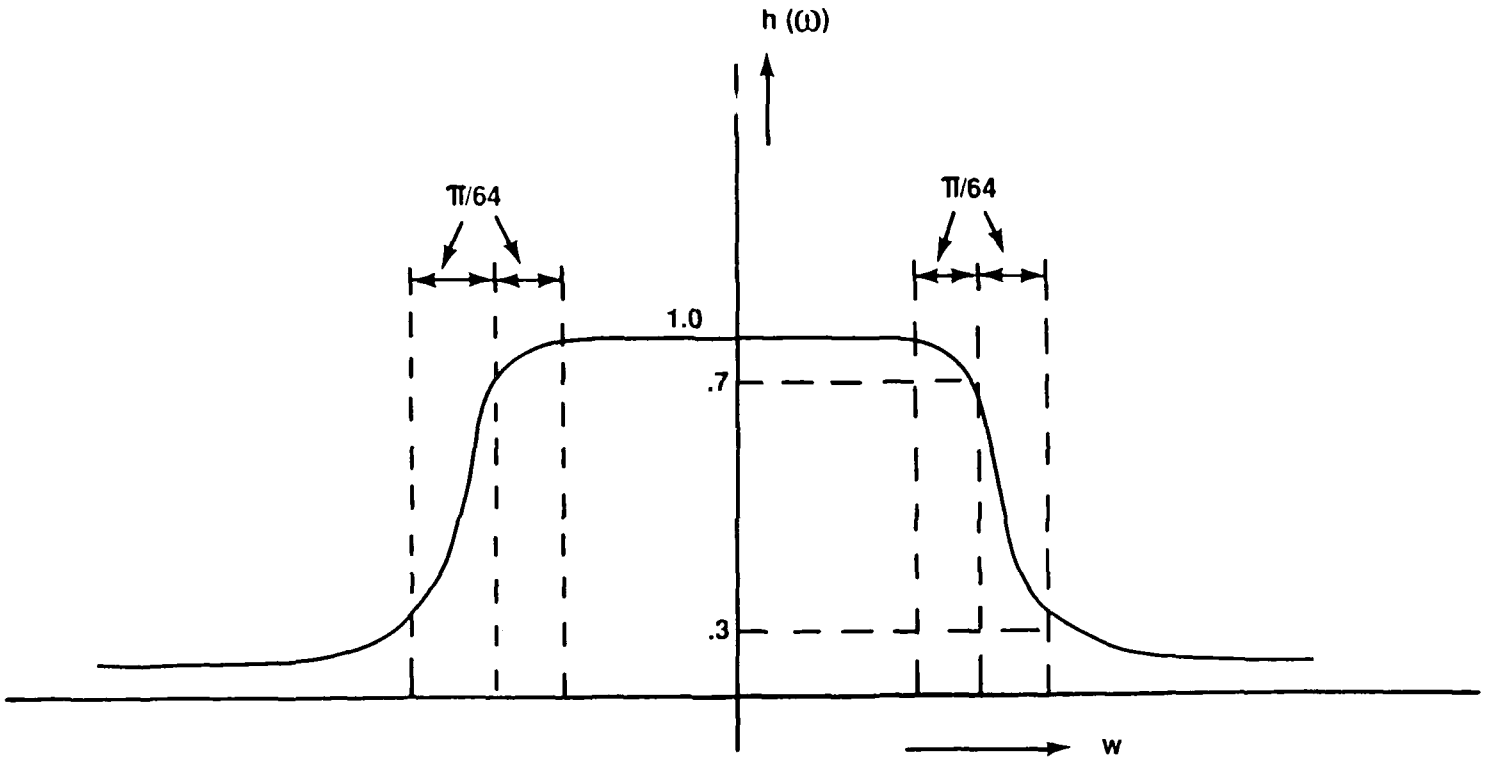

Figure 11. Frequency response of the low pass filter.

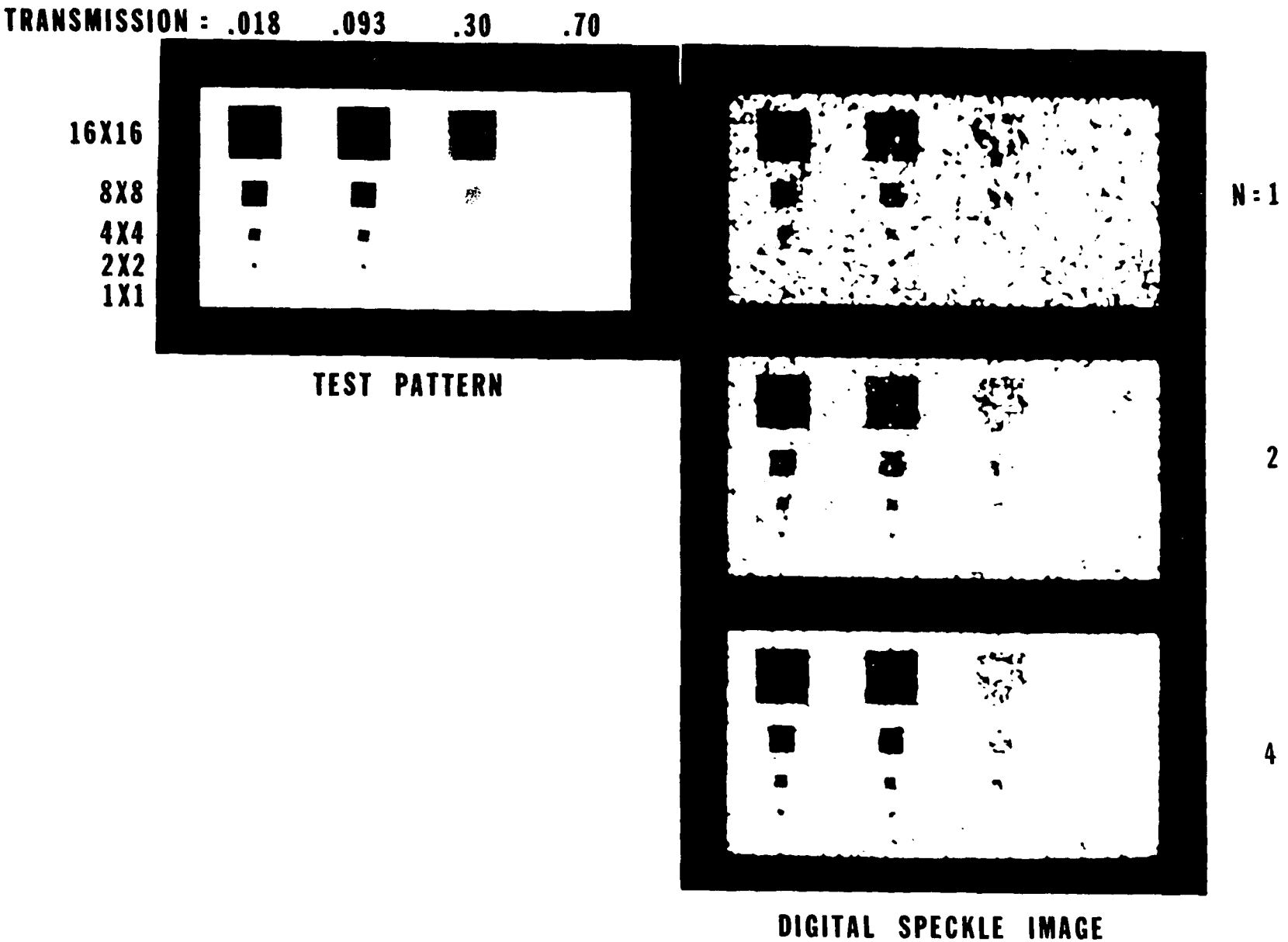

Figure 12. Test pattern and speckle images, N = 1,2,4.

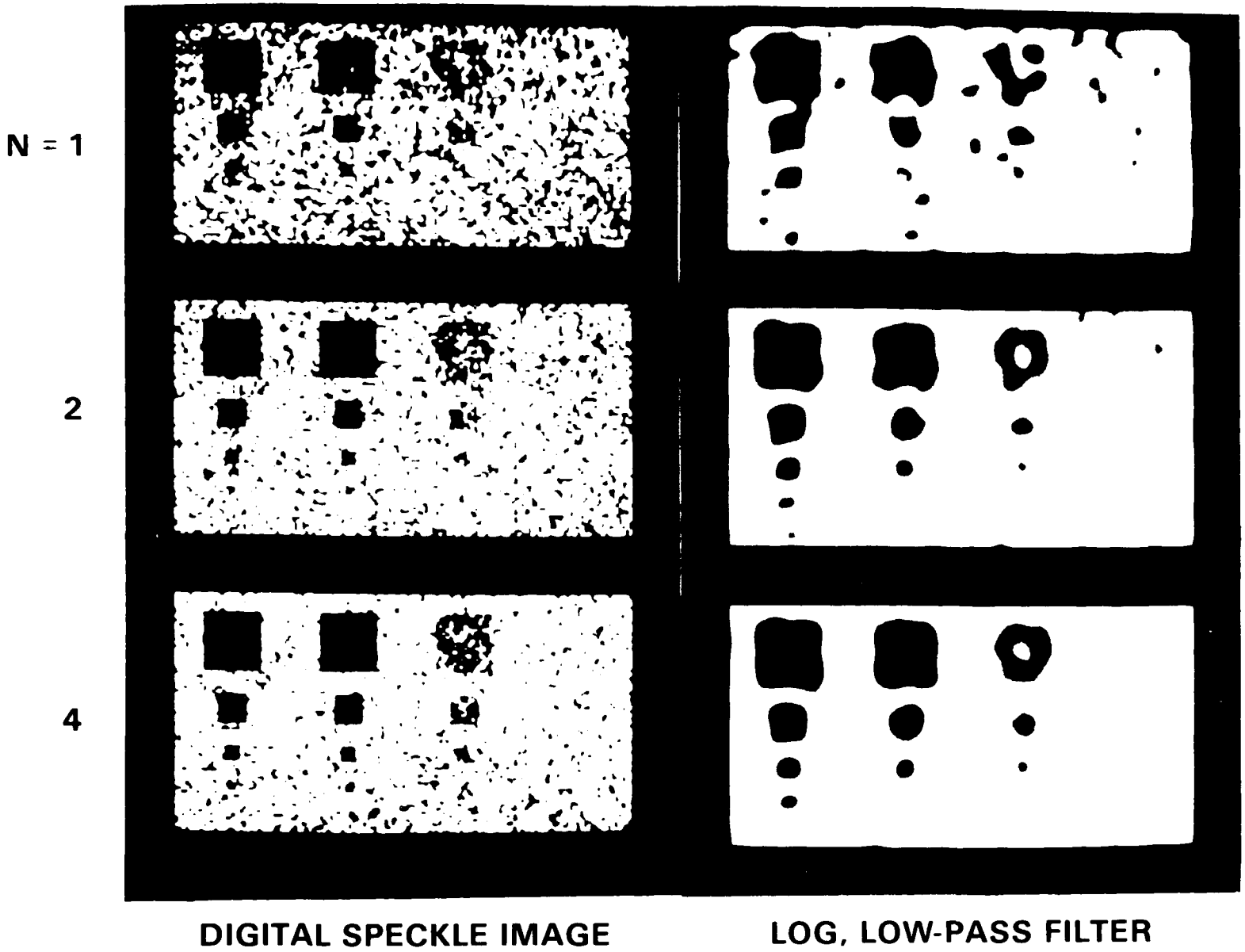

Figure 13. Homomorphic low pass filtering, N = 1,2,4.

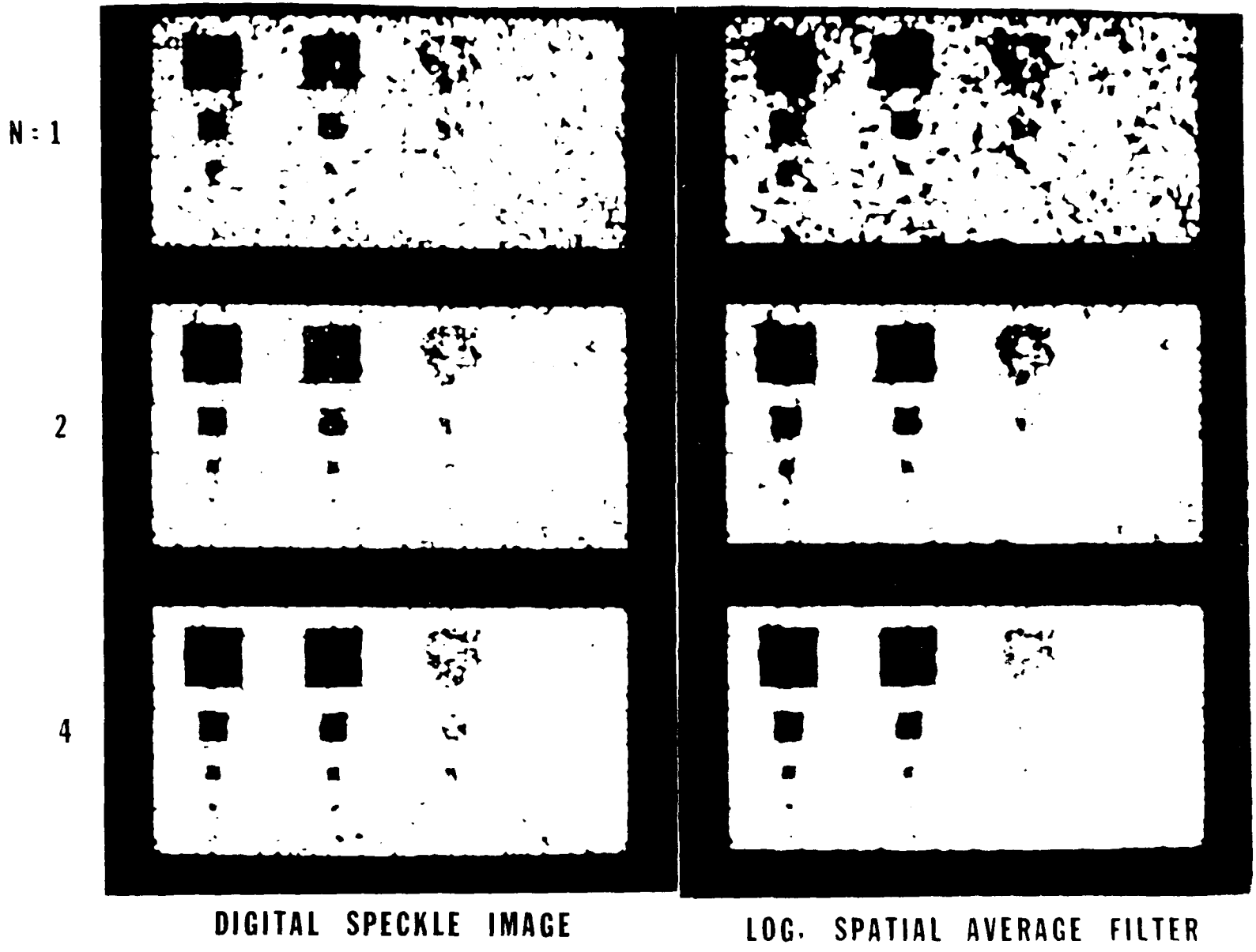

Figure 14. Homomorphic spatial averaging filter, N = 1,2,4.

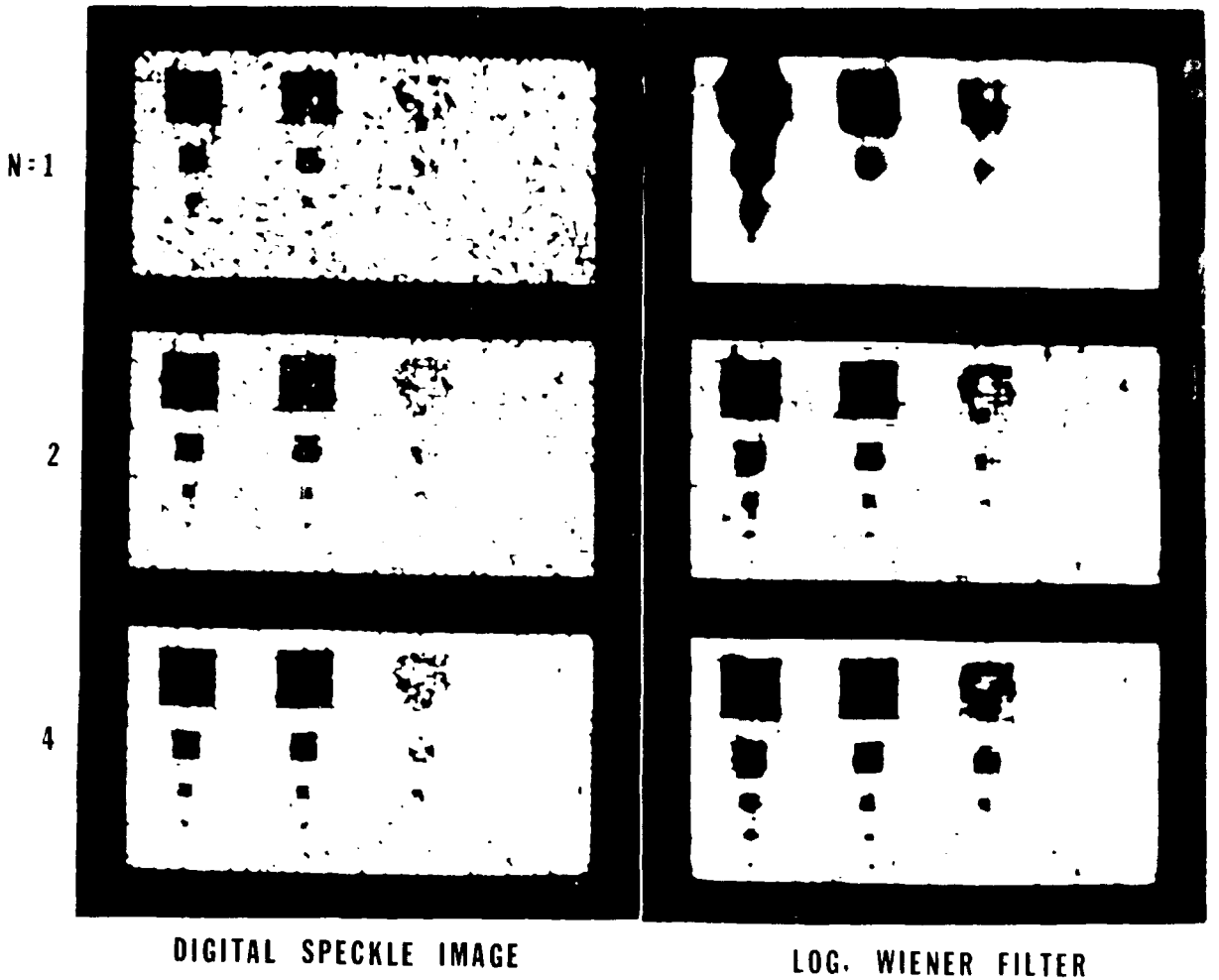

Figure 15. Homomorphic Wiener filter, N = 1,2,4.

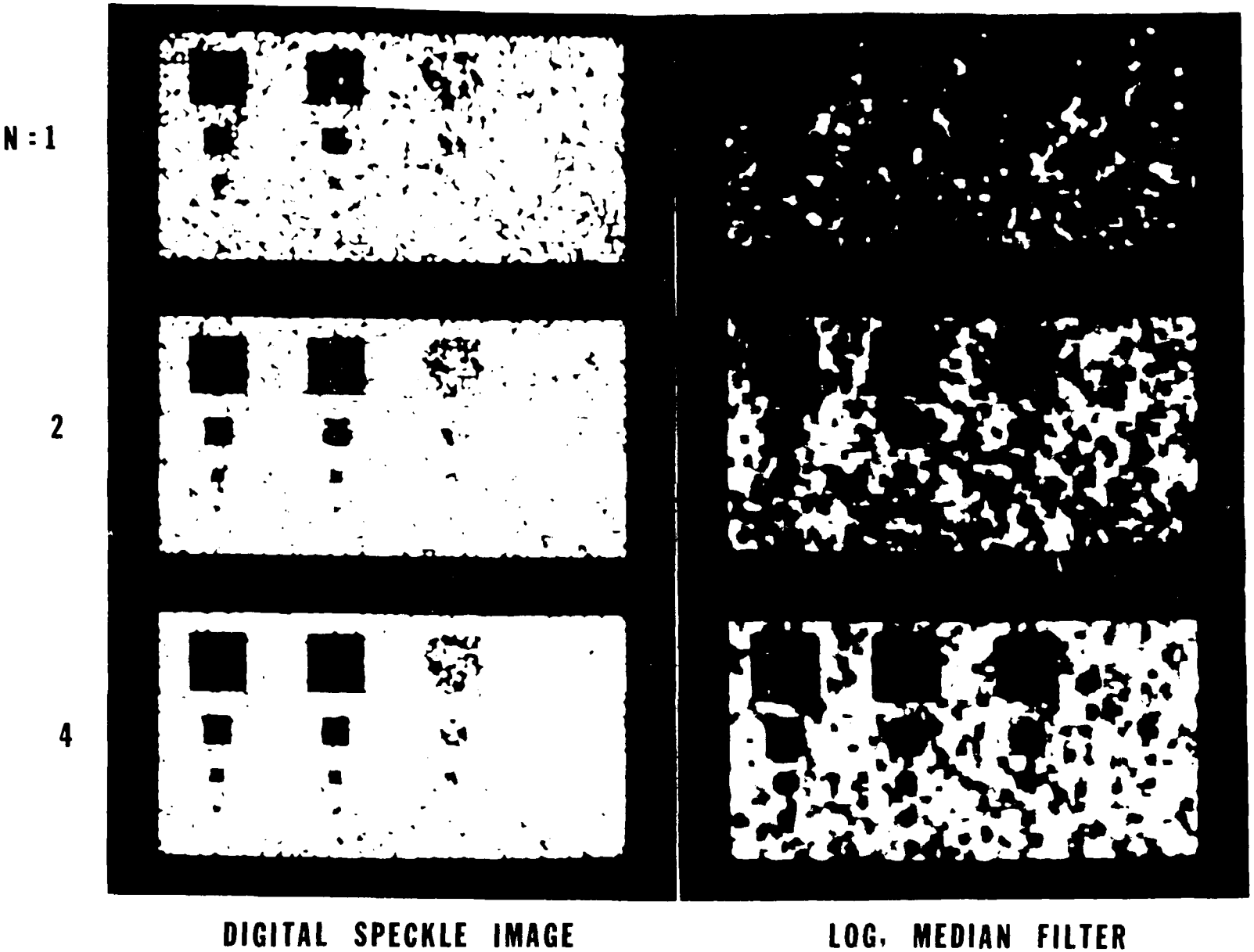

Figure 16. Homomorphic median filter, N = 1,2,4.

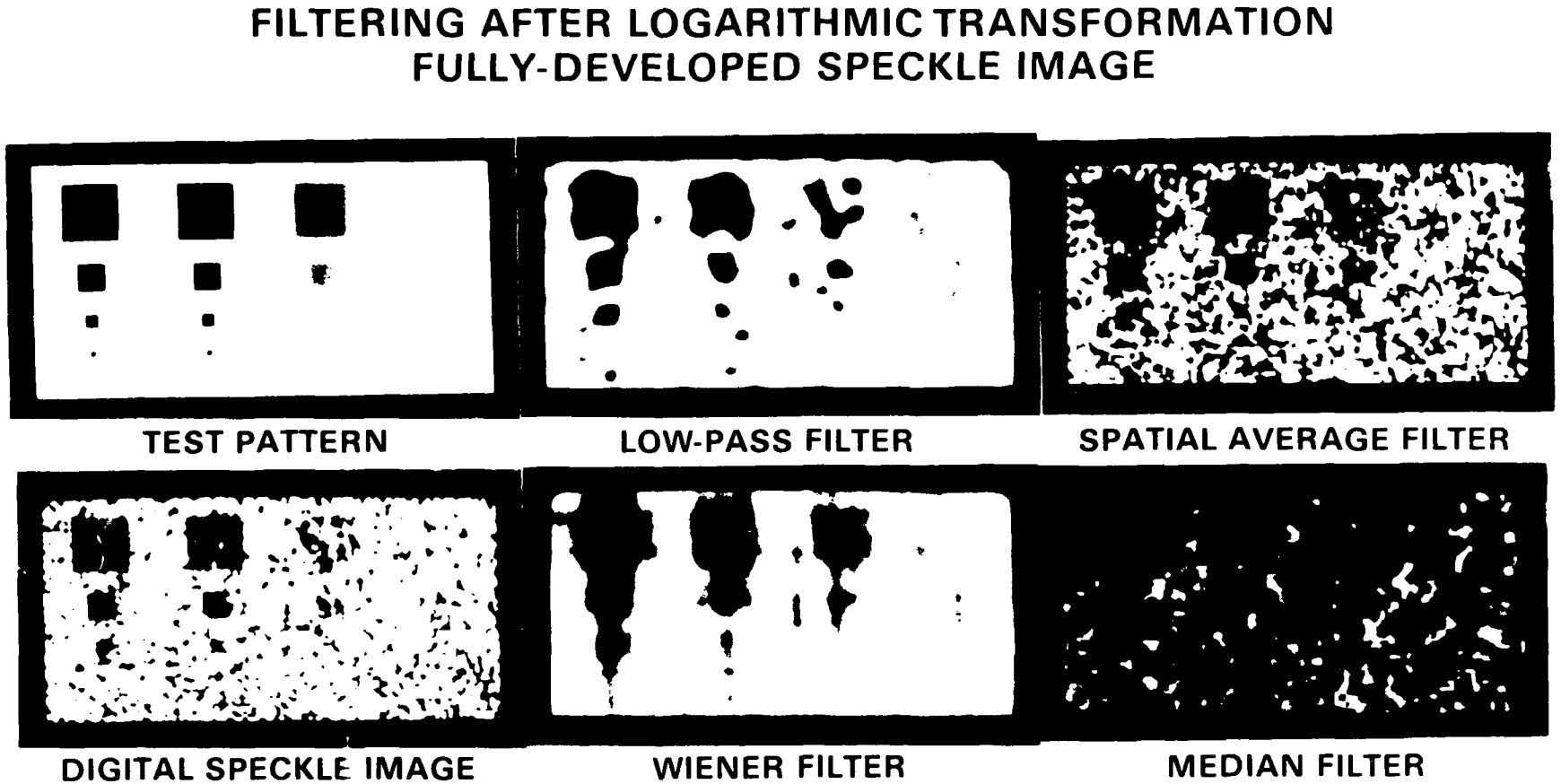

Figure 17. Comparison between various homomorphic filters, N = 1.

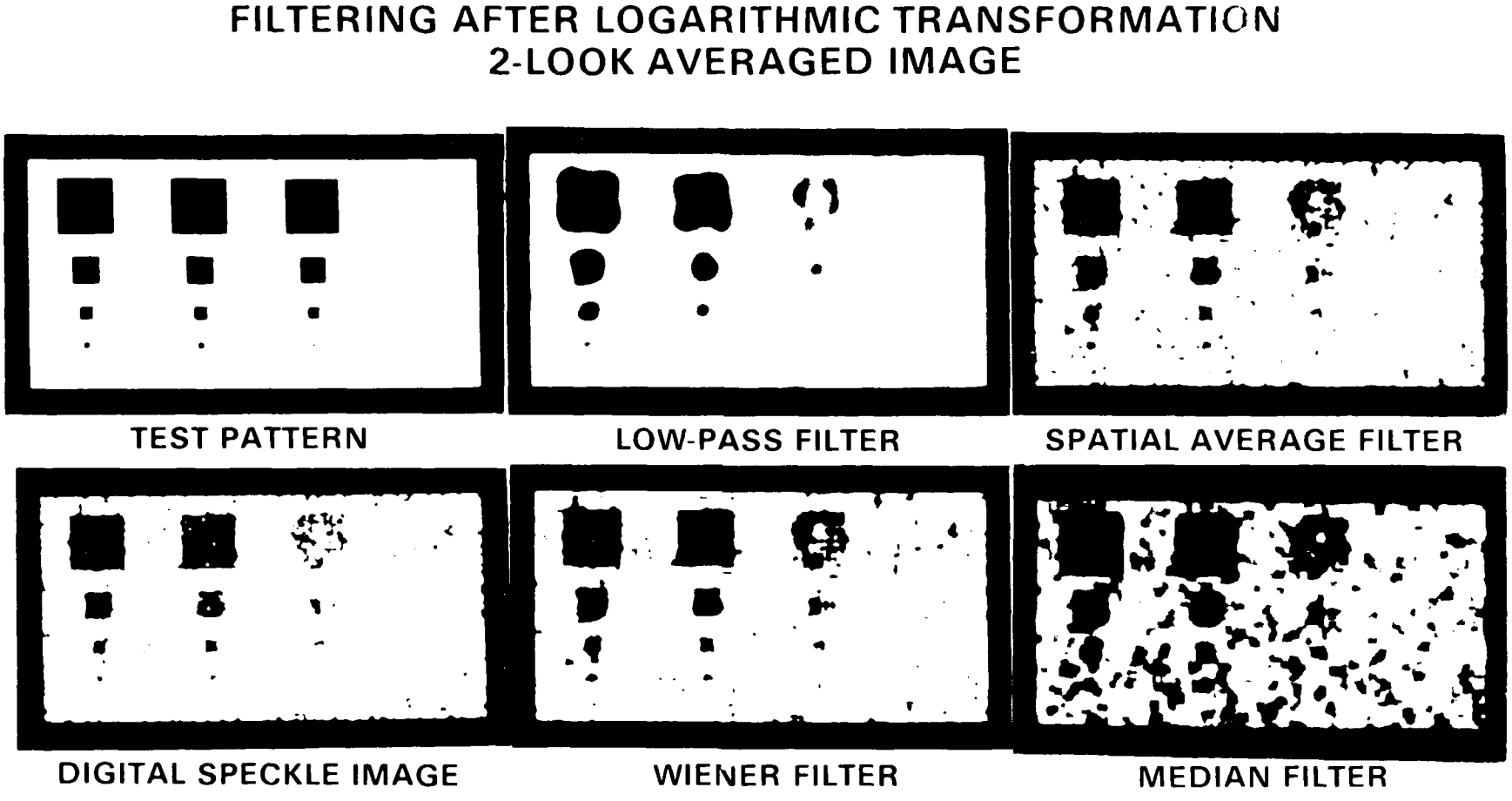

Figure 18. Comparison between various homomorphic filters, N = 2.

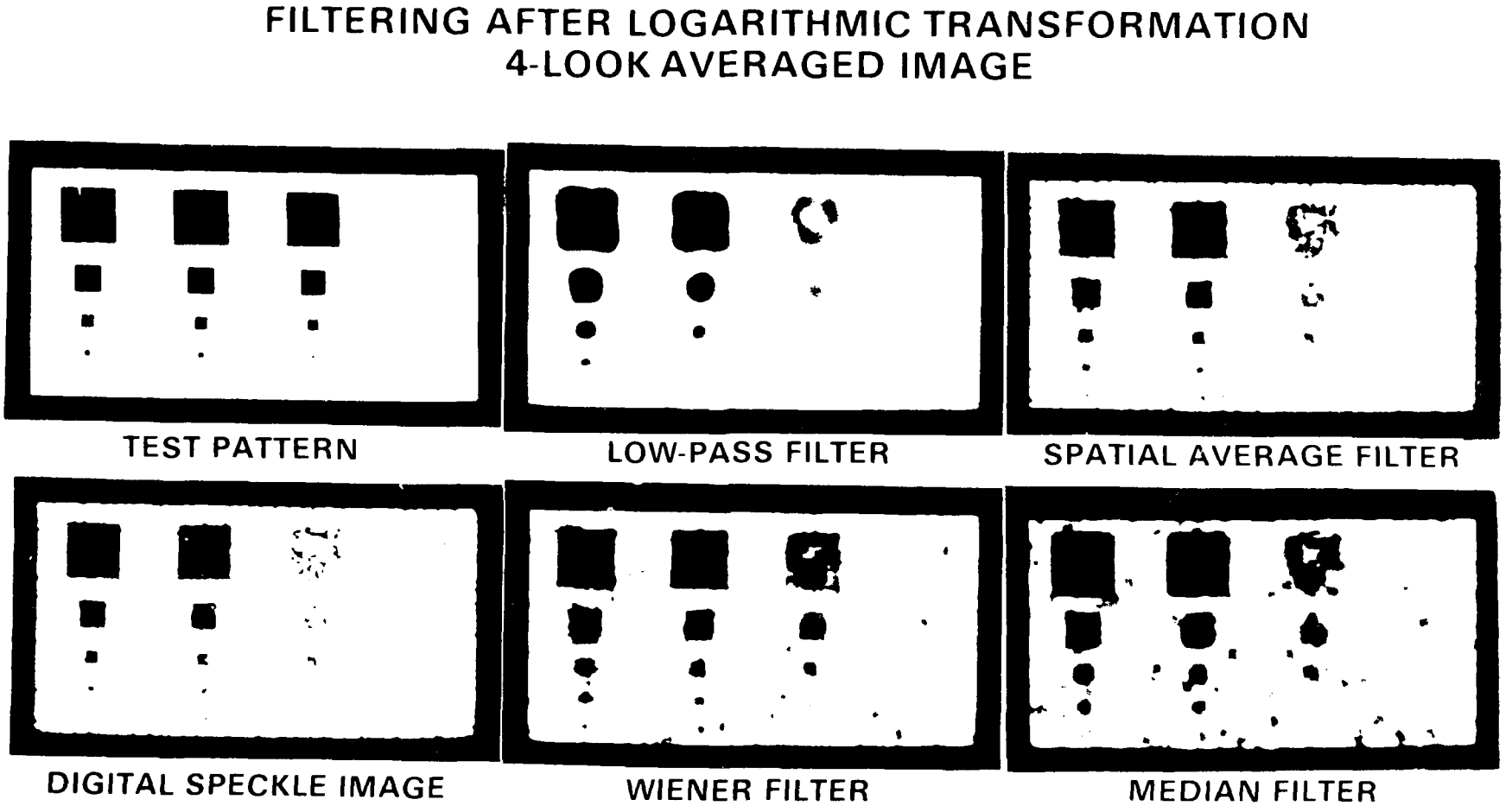

Figure 19. Comparison between various homomorphic filters, N = 4.

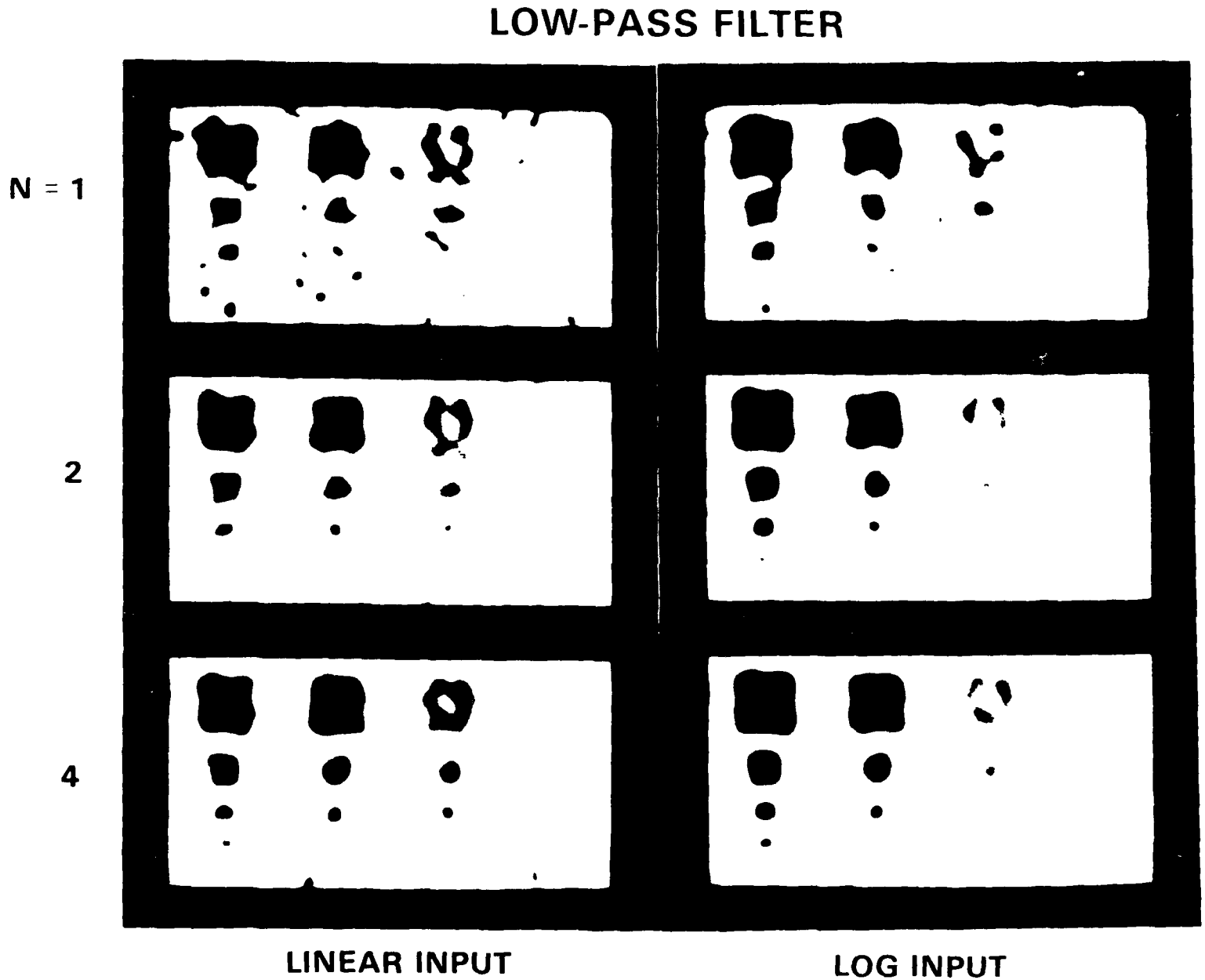

Figure 20. Comparison of linear and homomorphic low pass filters, N = 1,2,4.

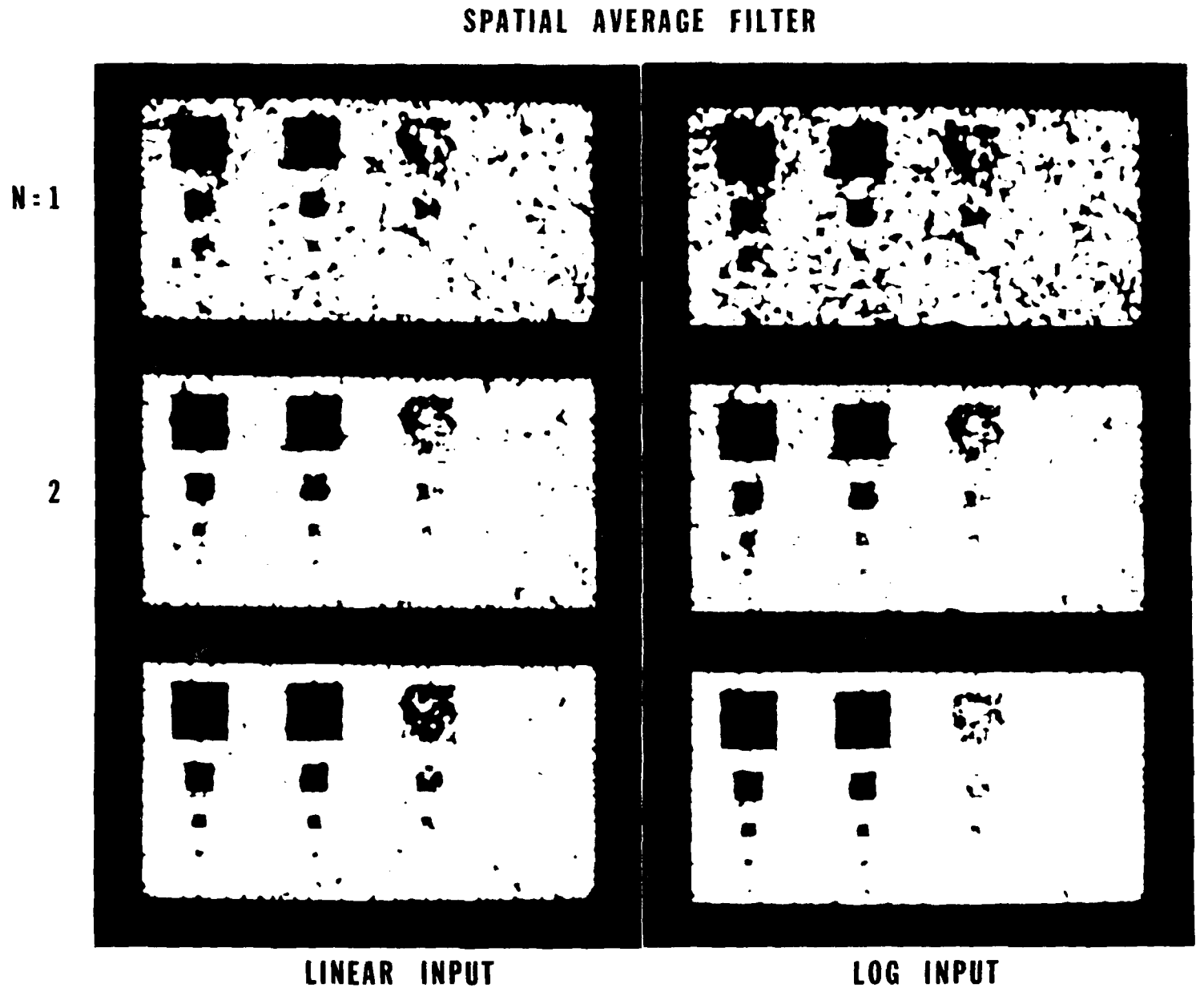

Figure 21. Comparison of linear and homomorphic spatial averaging filters, N = 1,2,4.

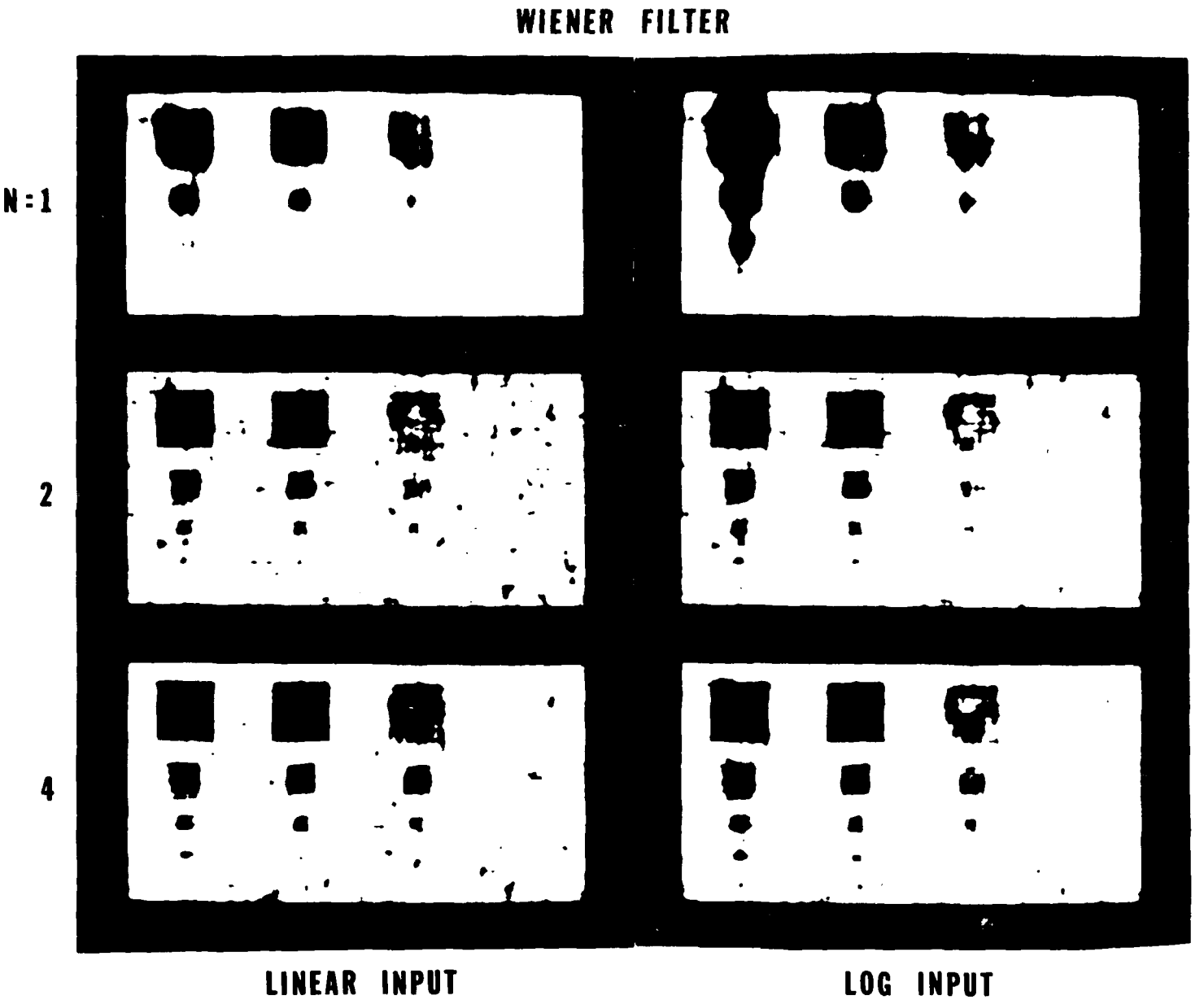

Figure 22. Comparison of linear and homomorphic Wiener filters, N = 1,2,4.

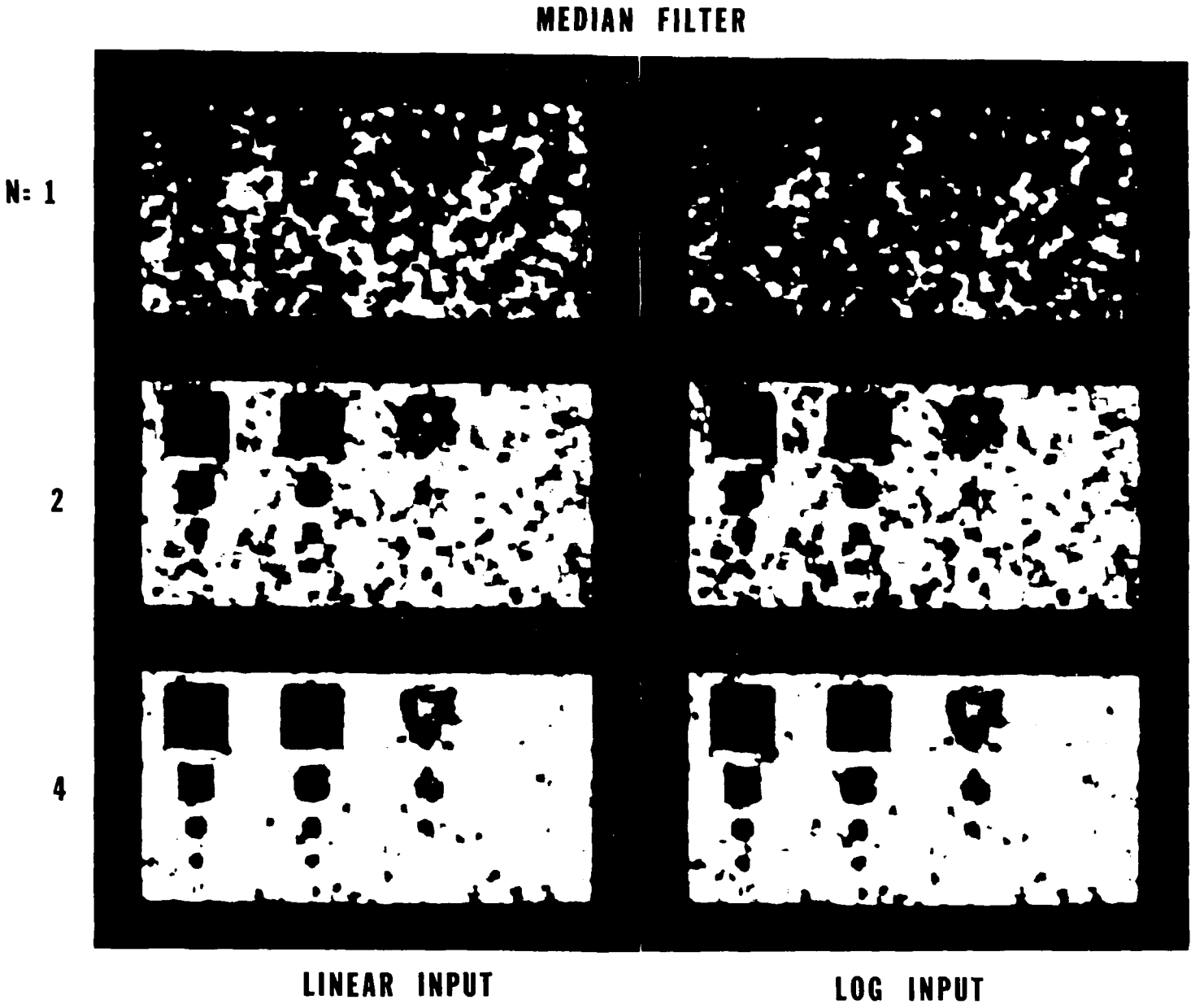

Figure 23. Comparison of linear and homomorphic median filters, N = 1,2,4.

REFERENCES

1. J. W. Goodman, "Statistical Properties of Laser Speckle Patterns," Laser Speckle and Related Phenomena, ed. J. C. Dainty (New York: Springer-Verlag, 1975).

2. J. Opt. Soc. Am. 66, No. 11 (Nov. 1976). The entire issue is devoted to "Speckle in Optics."

3. A. Kozma and C. R. Christensen, "The Effects of Speckle on Resolution," J. Opt. Soc. Am. 66 (1976), 1257-1260.

4. N. George, C. R. Christensen, J. S. Bennett, and B. D. Guenther, "Speckle Noise in Displays," J. Opt. Soc. Am. 66, (1976), 1282-1290.

5. J. C. Dainty, "Detection of Images Immersed in Speckle Noise," Opt. Octa. 18 (1971), 327-339.

6. H. Kato and J. W. Goodman, "Nonlinear filtering in coherent optical systems through halftone screen processes," Appl. Optics 14, (1975), 1813-1824.

7. A. Tai, T. Cheng and F. T. S. Yu, "Optical logarithmic filtering using inherent film nonlinearity," Applied Optics 16 (1977) p. 2559-

8. A. Rose, Vision, Human and Electronic (New York: Plenum Press) 1974.

9. B. D. Guenther, C. R. Christensen and A. K. Jain, "Digital Processing of Speckle Images," Proc. IEEE Conf. Pattern Recognition and Image Processing, 178 CH 1318-5C1, pp. 85-90, 1978.

10. C. R. Christensen, B. D. Guenther, J. S. Bennett, A. K. Jain, N. George and A. Kozma, "Object Detectability in Speckle Noise," Proc. SPIE Int. Conf. on Lasers, Orlando, FL, Dec 1978.

11. H. H. Arsenault and G. April, "Properties of Speckle Integrated with a Finite Aperture and Logarithmically Transformed," J. Opt. Soc. Am., Vol. 66, pp. 1160-1163, 1976.

12. A. K. Jain and C. R. Christensen, "Digital Processing of Images in Speckle Noise," Proceedings SPIE, Vol. 243, July 1980.

DISTRIBUTION

	No. of Copies
Director U.S. Army Research Office ATTN: SLCRO-PH SLCRO-ZC PO Box 12211 Research Triangle Park, NC 27709-2211	 1 1
Headquarters Department of the Army ATTN: DAMA-ARR Washington, DC 20310-0632	 1
Headquarters OUSDR&E ATTN: Dr. Ted Berlincourt The Pentagon Washington, DC 20310-0632	 1
Defense Advanced Research Projects Agency Defense Sciences Office Electronics Systems Division ATTN: Dr. John Neff 1400 Wilson Boulevard Arlington, VA 22209	 1
Commander U.S. Army Foreign Science and Technology Center ATTN: AIAST-RA 220 Seventh Street NE Charlottesville, VA 22901-5396	 1
Commander U.S. Army Strategic Defense Command ATTN: DASD-H-V PO Box 1500 Huntsville, AL 35807-3801	 1
Director, URI Univerity of Rochester College of Engineering and Applied Science The Institute of Optics Rochester, NY 14627	 1
Director, JSOP University of Arizona Optical Science Center Tucson, AZ 85721	 1

DISTRIBUTION (Concluded)

	No. of Copies
Dr. Anil K. Jain JMA, Inc. 517 Hubble Street Davis, CA 95616	100
U.S. Army Materiel System Analysis Activity ATTN: AMXSY-MP Aberdeen Proving Ground, MD 21005	1
IIT Resarch Institute ATTN: GACIAC 10 W. 35th Street Chicago, IL 60616	1
AMSMI-RD, Dr. McCorkle	1
Dr. Rhoades	1
-RD-RE, Dr. R. Hartman	1
Dr. J. Bennett	1
-RD-RE-OP, Dr. C. R. Christensen	100
-RD-CS-R	15
-RD-CS-T	1
-GC-IP, Mr. Fred Bush	1